Unravelling differential Hes1 dynamics during axis elongation of mouse embryos through single-cell tracking

Author list

Yasmine el Azhar[1], Pascal Schulthess[1, #], Marek J. van Oostrom[1, #], Wilke H.M. Meijer[1], Wouter M. Thomas[1], Marianne Bauer[2] and Katharina F. Sonnen[1,3,*]

Author affiliations

[1]Hubrecht Institute-KNAW (Royal Netherlands Academy of Arts and Sciences), University Medical Center Utrecht, Utrecht, The Netherlands

[2]Department of Bionanoscience, Kavli Institute of Nanoscience Delft, Technische Universiteit Delft, Van der Maasweg 9, 2629 HZ Delft, the Netherlands

[3]Lead contact

[#]These authors contributed equally.

*Correspondence: k.sonnen@hubrecht.eu

Summary

The intricate dynamics of Hes expression across diverse cell types in the developing vertebrate embryonic tail have remained elusive. To address this, we developed an endogenously tagged Hes1-Achilles mouse line, enabling precise quantification of dynamics at the single-cell resolution across various tissues. Our findings reveal striking disparities in Hes1 dynamics between presomitic mesoderm (PSM) and preneural tube (pre-NT) cells. While pre-NT cells display variable, low-amplitude oscillations, PSM cells exhibit synchronized, high-amplitude oscillations. Upon the induction of differentiation, the oscillation amplitude increases in pre-NT cells. Additionally, our study of Notch inhibition on Hes1 oscillations unveiled distinct responses in PSM and pre-NT cells, corresponding to differential Notch ligand expression dynamics. These findings suggest the involvement of separate mechanisms driving Hes1 oscillations. Thus, Hes1 demonstrates dynamic behaviour across adjacent tissues of the embryonic tail, yet the varying oscillation parameters give rise to differences in the information that can be conveyed by these dynamics.

Keywords

Signalling dynamics, protein dynamics, Notch, oscillations, bHLH genes, Hes1, somitogenesis, neuromesodermal progenitors, preneural tube, neural tube

Introduction

During embryonic development, tightly regulated cell fate decisions rely on intercellular communication. Recent insights indicate that cells encode information not only through the presence but also the dynamics of signalling pathways[1]. Oscillations in signalling pathways and target genes are widespread across tissues and developmental stages. Prominent among these are members of the hairy and enhancer of split (Hes) family of transcriptional repressors. Hes proteins, basic helix-loop-helix (bHLH) transcription factors, modulate gene expression by interacting with DNA as dimers[2]. Several of the seven Hes family members in mammalian cells are dynamically expressed in embryonic development[2-7].

During vertebrate development, neuromesodermal progenitors (NMPs) in the tailbud (TB) give rise to both the mesodermal and neural lineages, namely the presomitic mesoderm (PSM) and the neural tube (NT), respectively[8-10]. Hes dynamics play a critical role in the differentiation of both PSM and neural progenitors in the NT[3,11-13]. However, how Hes dynamics change during NMP differentiation is not understood. The periodic segmentation of the PSM into somites, known as somitogenesis, is driven by oscillatory signalling pathways, including FGF (fibroblast growth factor), Wnt (wingless and Int-1) and Notch signalling[4,14-18]. Whereas the exact composition of the segmentation clock differs per species, Notch signalling oscillations are found in all studied vertebrates, and several Notch target genes display oscillatory expression in PSM cells[4,17,19-22], including several members of the Hes gene family[4,13,23,24].

NMPs transitioning from the TB to the NT pass through the preneural tube (pre-NT), surrounded by oscillating PSM[25]. FGF signalling prevents premature differentiation in the pre-NT, while Notch signalling supports cell proliferation[26,27]. In the anterior NT, neural progenitor cells continue to proliferate and differentiate into future spinal cord neurons. Whether neural progenitor cells proliferate or differentiate has been linked to oscillations in Hes1 and Hes5, reminiscent of their function in somitogenesis[11,12]. Hes genes oscillate in progenitor cells to maintain a proliferative state[11,12,28-30], while sustained expression has been linked to quiescence[31,32]. Despite research into Hes dynamics in the anterior NT, investigations into Hes dynamics in NMPs and pre-NT are lacking.

In this study, we delineate the dynamics of Hes gene expression in mouse development and elucidate the signalling pathways orchestrating its expression during the differentiation of

neuromesodermal progenitors (NMPs) along neural and mesodermal trajectories. Leveraging a newly developed homozygously viable Hes1 reporter mouse line, generated through the endogenous tagging of the gene locus with a rapidly maturing yellow fluorescent protein, we thoroughly quantify Hes1 dynamics in the presomitic mesoderm (PSM), tailbud (TB), and preneural tube (pre-NT) regions of the embryonic tail. Through single-cell tracking, we discern distinct Hes1 dynamics between the PSM and pre-NT. Further investigation into Hes1 dynamics revealed disparate responses of PSM and pre-NT cells to signalling pathway perturbations. This also correlated with changes in proliferation. Thus, our new endogenous reporter mouse line, combined with recently available single-cell tracking software, allowed us to uncover previously unquantified dynamics in single cells of the mouse embryonic tail.

Results

Generation of a Hes1-Achilles mouse line to study signalling dynamics in the posterior embryonic tail

To investigate Hes dynamics in the developing mouse embryo, we first clarified which Hes genes were expressed in the PSM, NMP and in particular the pre-NT. The latter being defined as the tube-like Pax6-negative region emanating from the TB, which lies next to the PSM (Fig. 1A, B)[26,27]. To this end, we performed *in situ* hybridization (ISH) and hybridization chain reactions (HCR). Expression of Hes7 and Lfng (lunatic fringe), key components of the segmentation clock[24,33-36], was restricted to the PSM and TB or PSM, respectively (Fig. S1A, B, D). In contrast, both Hes1 and Hes5 were present in the TB, the PSM and the pre-NT with highest expression levels in the pre-NT and TB (Fig. 1C, S1C, D) (also see MAMEP database, http://mamep.molgen.mpg.de). Thus, both Hes1 and Hes5 are expressed in the different regions of the embryonic tail.

For further analysis into the dynamics of Hes genes, we then focused on Hes1, which shows a more localized expression to the neural lineage and PSM of the developing embryo than the ubiquitously expressed Hes5 (MAMEP database). To be able to quantify Hes1 expression levels over time, we generated a new endogenously tagged Hes1 mouse line (Fig. 1D-H). Building on previous approaches[31,37-40], we endogenously tagged Hes1 with Achilles, a fast-maturing fluorescent protein[38] (Fig. 1D, S2). We placed Achilles at the C-terminal side of Hes1 since this lies opposite to the DNA-binding bHLH (basic helix-loop-helix) domain of Hes1[2]. In addition, we separated Hes1 and Achilles by a flexible linker, because we reasoned that this should allow interaction of Hes1 via its C-terminal WRPW motif (four amino acid protein-protein interaction domain) with the Groucho/TLE family of transcriptional repressors[41,42]. Structure of the fusion protein was assessed for accessibility of the WRPW motif and bHLH

domain by Alphafold[43] (data not shown). Homozygous mice were born at Mendelian ratio (offspring of 8 heterozygous x heterozygous breedings: 17 wildtype, 34 heterozygous, 16 homozygous), viable and fertile. When comparing mRNA staining of Hes1 in wildtype embryos and Achilles in Hes1-Achilles embryos, the expression patterns corresponded (Fig. 1F, G). At protein level, Hes1-Achilles expression indicated the expected pattern with high expression levels in the pre-NT and stripes in forming somites (Fig. 1C, H). Thus, we successfully generated a homozygously viable, fertile and endogenous Hes1-Achilles reporter mouse line.

Hes1 expression is dependent on Notch signalling in the posterior embryonic tail

We next addressed whether Hes1 expression was solely dependent on Notch signalling or also on other pathways, as suggested previously for Hes7[39]. To be able to test this, we had to culture E10.5 embryonic tails *ex vivo* to quantify Hes1-Achilles dynamics upon pathway perturbation. However, standard embryo culture protocols[44,45] needed to be optimized for survival of the NT. Therefore, we optimised the protocol by testing different media to improve pre-NT and NT survival (Fig. 2A and data not shown). In standard embryo culture medium, cleaved caspase-3 expression levels especially in the pre-NT and NT were significantly higher than in uncultured embryos at embryonic day E11.5 (Fig. 2A, B). The tube was often filled with dead cells or disintegrated entirely. In contrast, in embryonic tails cultured in neurobasal medium (see further details in the Methods), the number of apoptotic cells was not increased compared to uncultured tails. Furthermore, the NT maintained its morphology and proliferative state (Fig. 2A, C). This suggests that the pre-NT is viable in the neurobasal medium. Despite this, somites were less well organized in neurobasal medium than in control samples (Fig. 2A). To find out whether culture conditions influenced the well-studied dynamics of the segmentation clock, we compared embryonic tails expressing LuVeLu[46] cultured in either embryo culture medium or neurobasal medium (Fig. S3A-D). Wave and oscillation dynamics as well as the regression of the oscillating field, a sign of differentiation, were similar between embryonic tails cultured in the different media (Fig. S3A, B). Accordingly, period and amplitude remained unchanged (Fig S3C, D). Thus, dynamics of the segmentation clock were maintained, and the optimized culture conditions of embryonic tails now allow the investigation of signalling dynamics in PSM, NMP and pre-NT *ex vivo*.

Using these culture conditions, we initially tested how pathway perturbation affected Hes1-Achilles expression levels. Notch inhibition, using the gamma-secretase inhibitor DAPT, led to a drop in Hes1-Achilles expression levels within 3 h (Fig. 2D, E). The dynamics and signal loss were comparable to the effect of Notch inhibition on the reporter Achilles-Hes7[38] (Fig. S3F, G). Besides Notch signalling, we also focused on Wnt (Fig. S3H-J) and FGF (Fig. S3K-

M) signalling, as gradients of these morphogens are present in the embryonic tail including the pre-NT (Fig. S3E). Accordingly, we found Dusp4 and Axin2, downstream targets of FGF and Wnt signalling, respectively, to be highly expressed in the pre-NT (Fig. S3H, K). We therefore perturbed embryonic tails with small molecules inhibiting these pathways: Wnt signalling was inhibited using the porcupine inhibitor IWP2 and FGF signalling was inhibited using SU5402, a small molecule inhibitor against the FGF receptor. Inhibiting either did not lead to a direct (IWP2) or consistent (SU5402) drop in signal, suggesting that these pathways might have more indirect effects on Hes1 expression levels. Thus, Hes1 expression in the posterior embryonic tail is driven by Notch signalling.

Population-wide Hes1 dynamics differ between TB, pre-NT and PSM

Subsequently, we carefully quantified Hes1-Achilles dynamics in the different regions of the embryonic tail (TB, PSM and pre-NT) (Fig. 3A-G, movie 1). We quantified dynamics in the TB region, which includes the NMPs but presumably also some posterior PSM cells. Every region significantly differed in expression level, in particular the pre-NT region showed higher Hes1-Achilles expression levels compared to the PSM region (Fig. 3H). In both the PSM and TB region, we detected oscillations over time (Fig. 3C, E). In contrast, Hes1-Achilles expression in the pre-NT region was dynamic, albeit noisier and showed less prominent oscillations over time compared to the other regions (Fig. 3G). When analysing the period using wavelet transform[47], there was a slight increase in periods in the TB region compared to PSM region (Fig. 3I). A similar trend towards an elevated period was observed for the pre-NT region. Furthermore, we found that the amplitude of the PSM region was significantly higher than in the pre-NT and TB regions (Fig. 3J). Finally, whereas kymographs revealed travelling waves of Hes1-Achilles expression levels in the PSM region (see * in kymograph), no clear tissue-wide pattern was detected in the pre-NT region (Fig. 3K). Overall, the data suggests that Hes1 is dynamic in the different regions of the mouse embryonic tail. However, Hes1 expression levels in the pre-NT are noisier and less oscillatory compared to the PSM.

Hes1 is oscillatory in single cells of the pre-NT

The fact that we did not find clear population-wide Hes1 oscillations or travelling waves in the pre-NT region could have different reasons: (1) There are no oscillations. (2) Single cells oscillate but are not synchronized with each other to induce tissue-wide oscillation dynamics. To test this, we performed a 2D spread-out experiment[45] combined with mosaic labelling of nuclei that allowed us to track cells individually and quantify Hes1-Achilles expression levels

170 in single cells (Fig. 4A-E, movie 2). When posterior embryonic tail tips are cultured on
171 fibronectin-coated dishes, the tissue spreads and cells, including those of the pre-NT, grow in
172 a quasi-monolayer, which facilitates single-cell tracking[45]. Immunostaining and HCR for neural
173 and mesodermal markers in 2D cultures confirmed presence and survival of PSM and neural
174 cell types, when culturing in neurobasal medium (Fig. S4A, B). As was observed in the
175 corresponding regions (Fig. 1,3), pre-NT cells showed higher Hes1-Achilles expression levels
176 than PSM cells, the latter of which slightly increased in intensity upon differentiation to somites
177 (Fig. 4F). Interestingly, oscillatory dynamics in Hes1-Achilles were found in both PSM and pre-
178 NT cells (Fig. 4B-E). Wavelet analysis indicated similar wavelet power distributions for PSM
179 and pre-NT cells (data not shown). Likewise, the periods and amplitudes were similar, even
180 though the amplitudes in pre-NT cells were slightly reduced (Fig. 4G, H). The discrepancy
181 between amplitude at population (Fig. 3) and single-cell level (Fig. 4H) supports the hypothesis
182 that Hes1 dynamics are not synchronized between neighbouring pre-NT cells.

183 Using Fourier transform to analyse the dynamics, similar periods were obtained (Fig. 4I, J,
184 S4C-E). Comparison of Fourier spectra of individual cells indicated that Hes1-Achilles
185 dynamics were noisier in pre-NT than PSM cells, since PSM cells mostly showed one main
186 peak at 2.5 h and pre-NT cells multiple peaks around 2-4 h (Fig. 4I, J). As a measure of
187 variability, we determined the full width at half maximum (FWHM) for the period quantification
188 (Fig. S4E), which was 0.5 for the PSM and 1.6 for the pre-NT. The coefficient of variation was
189 0.1 and 0.2 for PSM and pre-NT cells, respectively. Thus, like PSM cells, single cells in the
190 pre-NT show Hes1 oscillations. However, oscillations are more variable and not synchronized
191 between neighbouring cells.

192

193 **Hes1 shows oscillations in NMPs that are driven by Notch signalling**

194 After the discovery of Hes1 dynamics in both PSM and pre-NT cells, we next sought to quantify
195 Hes1 dynamics in NMPs, from which both PSM and pre-NT arise. The 2D spread-out
196 experiments (Figure 4) did not allow us to unequivocally identify NMPs. Therefore, we
197 analysed Hes1-Achilles dynamics in NMPs by *in vitro* differentiation. To this end, we applied a
198 previously published NMP differentiation protocol (Fig. 5A)[48] to generate NMPs from
199 embryonic stem cells (ESCs) derived from Hes1-Achilles mice (Fig. 1E). To identify embryonic
200 and neural fate, while quantifying Hes1-Achilles expression levels over time, we added a
201 Sox2-H2B-iRFP reporter ("Sox2-iRFP") into Hes1-Achilles cells by endogenously tagging
202 Sox2 using CRISPaint[49]. Based on previous literature and immunostainings, we defined the
203 NMP phase between 56 and 72 hours (Fig. 5A, S5A)[48,50]. When analysing Hes1-Achilles
204 dynamics at population level, oscillations resembled in appearance and amplitude that of the

205 TB region of the *ex vivo* embryonic tail, albeit with a reduced period (Fig. 5B-E, 3D, E). To find
206 out if single cells show Hes1 oscillations, we next tracked single NMP cells and quantified
207 Hes1-Achilles dynamics (Fig. 5F-I). Hes1-Achilles expression was dynamic in NMPs with a
208 period of around 2.5 h (Fig. 5H). The oscillations were variable and had a low amplitude (Fig.
209 5G, I). When perturbing Notch signalling using the inhibitor DAPT, we detected a dose-
210 dependent decrease of Hes1-Achilles expression levels (Fig. S5B-E). This inhibition did not
211 show an apparent effect on the period or amplitude of Hes1-Achilles dynamics. Furthermore,
212 when we differentiated NMPs further towards the mesodermal or neural lineage (Fig. S5F-P),
213 cells displayed dynamics corresponding to those found *ex vivo* (Fig. 3). Thus, NMPs show
214 variable oscillations in Hes1 expression levels that are dependent on Notch signalling.

215

216 **Induced differentiation to neural tube by FGF inhibition results in Hes1 dynamics with**
217 **increased amplitude in the pre-NT**

218 Previous studies have highlighted the function of Hes dynamics in the anterior NT[6,13,28,29,32,51].
219 Therefore, we asked how Hes1 dynamics changed upon induced differentiation. Since FGF
220 inhibition induces differentiation of pre-NT to NT[25,27,52] and PSM to somite[53,54], we inhibited
221 FGF activity in 2D spread-out cultures using SU5402 (Fig. 6). As expected, FGF inhibition led
222 to a rapid regression of the oscillating field in the PSM, which indicated induced differentiation
223 and confirmed effectiveness of the inhibitor (Fig. S6A). In agreement with changes of Hes1
224 expression levels from 'posterior' to 'anterior' PSM (Fig. 4F), Hes1-Achilles expression levels
225 were increased in the PSM region upon FGF inhibition, while period and amplitude remained
226 unchanged (Fig. S6B-D). Conversely, we did detect a decrease in Hes1-Achilles amplitude in
227 the pre-NT region upon FGF inhibition (Fig. S6E-G).

228 To investigate the effect of FGF inhibition on single cell oscillations, we then performed single-
229 cell tracking. In PSM cells FGF inhibition had a similar effect on Hes1-Achilles dynamics as at
230 population level with increased absolute expression levels and a corresponding increase in
231 amplitude, i.e. the relative amplitude remained unchanged, while the period was maintained
232 (Fig. S6H-J). In contrast, FGF signalling inhibition had a different effect on Hes1-Achilles
233 dynamics in pre-NT cells: absolute expression levels of Hes1-Achilles and the oscillation
234 period remained similar (Fig. 6A-D, S6K, L), whereas the relative amplitude of Hes1-Achilles
235 dynamics increased (Fig. 6E, S6M). It has been shown recently that expression of the Notch
236 ligand Dll1 begins to oscillate in the NT, adjacent to the last formed somites[11]. To test if
237 differentiation induced by FGF inhibition might have led to changes in Dll1 expression in 2D
238 cultures, we quantified Dll1 by immunostainings. However, we did not detect changes in Dll1
239 expression levels in the Sox2-positive cell population upon FGF inhibition (Fig. 6F, G, S6N).

240 Thus, this suggests that high FGF signalling levels in pre-NT cells have a dampening effect
241 on Hes1 oscillations and that differentiation leads to an increase in oscillation amplitude, which
242 is not dependent on overall Dll1 protein expression levels.

243

244 **Changing Hes1 dynamics by modulating Notch signalling correlates with an increase**
245 **in cell proliferation**

246 We next addressed if a common mechanism drives Hes1 oscillations in cells of the different
247 tissue types. In general, a delayed negative feedback loop has been suggested to drive such
248 oscillations via repression of Hes genes by Hes proteins themselves[13,24,35,55-58]. In addition to
249 a Hes-driven feedback loop, the Notch ligand Dll1 is dynamically expressed in the PSM[11,59],
250 which has been proposed to drive a delayed coupling mechanism of segmentation clock
251 oscillations resulting in kinematic waves in the PSM[38,59-61]. In neural tissue, however, Dll1
252 oscillations were not observed in the pre-NT, but only in the NT adjacent to the last formed
253 somites, where single cells started to oscillate in a salt-and-pepper like pattern[11]. Thus, to
254 clarify the role of Notch signalling in driving Hes1 oscillations in the embryonic tail, we first
255 analysed the expression of Notch signalling components in the different regions of the
256 embryonic tail, especially the pre-NT. We found Delta-like (Dll) Notch ligands Dll1, Dll3 and
257 Dll4 and the Notch receptors to be expressed in the PSM, TB and pre-NT by HCR[62] (Fig. S7A,
258 B). We next performed immunostainings to visualize ligand protein expression levels. In
259 agreement with previous publications[11], Dll1 expression levels were elevated in the PSM
260 compared to the pre-NT and staining patterns varied between embryonic tails indicating
261 dynamic expression (Fig. 7A and data not shown). However, Dll1 – just like Dll4 – was not only
262 detected in the PSM but also in the pre-NT and TB, albeit at lower expression levels and
263 without indications of dynamics (Fig. 7A). Together with previous findings on Dll1 oscillations
264 in the embryonic tail[11], this suggests that Dll1 and Dll4 are present at low expression levels in
265 pre-NT cells but not oscillatory, whereas Dll1 expression levels oscillate in PSM cells (Fig. 7B).

266 To compare the influence of Notch signalling on Hes1 protein dynamics in PSM and pre-NT
267 cells, we inhibited Notch signalling with different doses of DAPT and quantified Hes1-Achilles
268 dynamics within PSM and pre-NT at population level and in single cells (Fig. 7, S7). Analysing
269 dynamics in PSM at population level, we found that Hes1-Achilles levels decreased to a similar
270 extent for all DAPT concentrations used (Fig. S7C). The oscillation period was slightly
271 increased at 1 μM DAPT, however the amplitude was strongly reduced independent of the
272 DAPT concentration used (Fig. S7D, E). This indicates that at population level, Notch inhibition
273 leads to a loss of Hes1-Achilles oscillations in the PSM even at low concentrations, which
274 could be consistent with a loss in synchrony between neighbouring cells. In contrast, in pre-

NT (Fig. S7F-H) Notch inhibition led to dose-dependent decrease in Hes1-Achilles levels (Fig. S7F) and amplitude, which was only significant at 10 μM DAPT (Fig. S7H).

To clarify how Notch inhibition affects single-cell oscillations, we performed single-cell tracking and quantified Hes1-Achilles levels in PSM in the different conditions. Also, at single-cell level, Notch inhibition led to a dose-dependent decrease of Hes1-Achilles levels in pre-NT cells (Fig. 7C-E, S7I-K). This correlated with a corresponding decrease in oscillation amplitude with the relative amplitude remaining unchanged (Fig. 7G, S7K). However, no significant change in period was observed (Fig. 7F, S7J). Conversely, in PSM cells Notch inhibition led to a decrease in both Hes1-Achilles expression levels and the relative amplitude (Fig. 7C-G, S7L-N). Likewise, the Hes1-Achilles oscillation period was decreased with high DAPT concentration (Fig. 7F). Thus, Notch inhibition has differential effects on Hes1 oscillations in the PSM and pre-NT, which implies that the mechanism driving Hes1 dynamics differs between the two cell types.

While the essential function of Notch signalling in somitogenesis has been studied extensively[63-66], its role in the pre-NT especially with regards to signalling dynamics is less clear, even though it has been implicated in cell proliferation control[26]. In other regions of the nervous system, Hes1 oscillations also regulate proliferation with high, sustained Hes1 expression levels promoting quiescence[31,32,67]. We therefore addressed how Notch signalling inhibition and a corresponding modulation of Hes1-Achilles dynamics affected pre-NT proliferation. Interestingly, when quantifying the percentage of phospho-histone H3-positive mitotic cells in the Sox2-positive region (mitotic index), we found that Notch inhibition led to an increase in the mitotic index (Fig 7F, G, S7O). This suggests that lowering Notch signalling and thereby Hes1 expression levels and oscillation amplitude, while leaving the period unchanged, promotes proliferation in the pre-NT.

Discussion

Here, we have addressed how Hes dynamics change in the context of the developing embryonic tail, in particular focussing on the tissues derived from NMPs. To enable this, we have generated a new and endogenous Hes1 reporter mouse line. It contains the fast-maturing fluorescent protein Achilles, which is placed C-terminally to the Hes1 gene. Importantly, the line is homozygously viable and fertile and allows the investigation of Hes1 dynamics at single-cell resolution in various tissue types (Sonnen, unpublished). Using this new reporter, we compared Hes1 dynamics in the PSM and pre-NT at population and single-cell level.

To make this feasible, we had to optimize the embryonic tail culture protocol to ensure survival of NT cells during *ex vivo* culture. In contrast to the minimal DMEM-F-12 medium which is optimal for PSM growth and differentiation[68], we made use of neurobasal medium which is optimized for culture of neural tissues. The latter is not only supplemented with additional nutrients and vitamins, but also contains proteins such as insulin. Which of these components are required for NT and pre-NT survival must be addressed in future studies. While this medium allows NT survival, we do observe morphological defects in somite formation, which are presumably due to the presence of retinoic acid in the medium. Despite these morphological defects, dynamics of the segmentation clock are maintained. This medium therefore allowed us to culture embryonic tails *ex vivo* for the quantification of signalling dynamics in both tissue types in the same culture.

Differential mechanisms driving Hes1 dynamics in the PSM and pre-NT

In pre-NT cells, Hes1 oscillated at high expression levels with low amplitude, whereas in PSM cells, it oscillated at low expression levels with high amplitude (Figure 7H). Notch inhibition led to a decrease in Hes1 expression levels and a proportional decrease in the amplitude in pre-NT cells. In contrast, in PSM cells an over-proportional decrease in amplitude was induced, i.e. the relative amplitude decreased, both when analysing Hes dynamics at population and single-cell level. This implies that different mechanisms drive Hes1 dynamics in the two tissue types. While the effect of Notch inhibition on Hes1 dynamics in pre-NT cells is consistent with a delayed negative feedback loop downstream of constant Notch signalling[55,56], oscillations in PSM cells appear to be further amplified in a Notch-dependent manner.

In fact, the Notch ligand Dll1 has been shown to oscillate in various cell types including the PSM, which results in periodic activation of proneural gene expression[11,69,70]. Previously, Dll1 oscillations were not detected in the pre-NT, but only in the NT adjacent to the somites[11]. We have shown here that even in the pre-NT both Dll1 and Dll4 are present at low expression levels. Interestingly, in a study using cultured cancer cell lines it was shown that Dll1 expression induces dynamic expression, while Dll4 leads to more sustained expression of downstream target genes[71]. How the presence of each ligand and the dynamics of Dll1 exactly influence Hes1 dynamics in PSM and pre-NT cells has to be addressed in future studies.

In the PSM, oscillatory Dll1 expression has been suggested to lead to kinematic waves travelling through the PSM[11,61,72]. Loss of Notch-dependant intercellular coupling could therefore explain the loss of population-wide dynamics we observed already at low Notch inhibitor concentrations. However, the oscillation amplitude was also reduced in single cell oscillations upon Notch inhibition arguing against a sole effect on synchronicity between

oscillators. The fact that high Notch inhibitor levels also led to a decrease in the relative Hes1 oscillation amplitude in the pre-NT at population level suggests that Notch signalling might induce some form of synchronization between pre-NT cells, as suggested recently for Hes5 in the NT[73]. Our mosaic labelling approach for single-cell tracking does not allow us to quantify Hes1 dynamics in neighbouring cells, which might be studied further in the future.

Implications for the role of Hes1 dynamics in the preneural tube

Hes1 dynamics have been found to regulate proliferation and differentiation in the anterior developing NT[13,67,74]. In undifferentiated cells, Hes1 oscillates in an alternating fashion with proneural genes, while Hes1 is switched off in differentiating cells. Moreover, high absolute expression levels regulate the switch between quiescence and proliferation in adult stem cells with high expression levels maintaining a quiescent state[31,32,67]. It is therefore interesting to note that we find Hes1 expression levels highest in the pre-NT and expression decreases towards the NT. When inducing a decrease in Hes1 expression levels and oscillation amplitude by inhibiting Notch signalling, the mitotic index was indeed increased. Similar to morphogen gradients in the PSM, FGF and Wnt signalling are high in the pre-NT. High FGF signalling prevents differentiation of the pre-NT to NT[25,27,52-54]. By quantifying Hes1 dynamics in pre-NT cells upon inhibition of FGF signalling, we found that the amplitude of Hes1 dynamics was increased (Fig. 7H). This indicates that FGF has a dampening effect on Hes1 dynamics in the pre-NT and that reduced FGF signalling results in Hes1 dynamics with higher amplitude. Whether FGF signalling directly affects Hes1 dynamics or functions indirectly via induction of differentiation has to be disentangled in the future.

Together, this supports a hypothesis in which cells in the pre-NT are maintained in an undifferentiated, waiting phase until they become part of the NT, where cells differentiate further in conjunction with the neighbouring somites.

Information transmission by noisy Hes1 oscillations

We have quantified Hes1 oscillations in single PSM, NMP and pre-NT cells. In both NMP and pre-NT cells, Hes1 oscillations are noisy at high expression level with low amplitude. In contrast, in the PSM single-cell oscillations are less noisy at low expression level with higher amplitude (Fig. 7H). In addition to these single-cell oscillations, it is well known that oscillations between neighbouring PSM cells are coupled leading to travelling waves of signalling along the tissue[40,46,75]. These coupled, highly synchronized oscillations ensure that information for proper segmentation can be transmitted from posterior to anterior in every segmentation cycle.

Even though the pre-NT lies directly adjacent to this oscillating field, the tissues are spatially separated by epithelialization and extracellular material. In the TB and pre-NT, we detect different expression patterns of several signalling components and downstream targets of the Wnt and Notch signalling pathway compared to the PSM (this study and MAMEP database). In correlation with this, Hes1 dynamics in pre-NT cells and NMPs are not only noisy but also less synchronized between neighbouring cells. The absence of synchronized oscillations or travelling waves implies that information in the pre-NT is not transmitted along the anterior-posterior axis via these dynamics. Conversely, Hes1 presumably has a more local function in regulating cellular behaviour on a single-cell basis, as has been suggested in other tissues[69,70].

Notably, once the pre-NT has differentiated to the NT, it has been shown that signalling between somite and NT does regulate further patterning and segmentation of the developing NT in conjunction with the differentiating somite[76]. This ensures that spinal cord, nerves and vertebrae form one unit. Thus, proper patterning of the embryo's spinal axis would be dependent on proper somitogenesis. Based on this, somitogenesis would therefore have to be tightly regulated and coupled to axial elongation, which necessitates highly accurate information transmission. In contrast, differentiation and segmentation of the NT would be downstream of somite formation, which suggests that information could be kept local with the sole aim to allow proliferation and prevent faulty or premature differentiation of single cells in the pre-NT.

In summary, Notch-dependent Hes1 dynamics in single cells of the developing embryonic tail differ in expression levels, amplitude and noise, which has implications for information transmission in the PSM and NT. The detailed molecular mechanism of how Hes dynamics are generated and what information is stored in these dynamics in different cell types during embryonic development are important questions for future studies.

Acknowledgements

We thank all members of the Sonnen, Bothma and Garaycoechea labs for feedback and discussions. We are thankful to Juan Garaycoechea and Jacques Bothma for feedback on the manuscript. We thank Jan-Daniël de Leede for help with data analysis, Valerie Wilson, Mina Gouti and Jana Wolf for useful discussions and Andreas Sonnen for help with Alphafold. We thank Jeroen Korving, Stieneke van den Brink, Joris Geigenmüller, Tjerk Swinkels and Mariska Dijkers for technical help. This work was supported by the Hubrecht imaging and animal facilities. The H2B-mCherry was kindly provided by the Riken Center for Biosystems Dynamics Research. The T-Cre/ERT2, RosaCreERT and PGK-Cre lines were kindly provided by Jackson Laboratories. The LuVeLu reporter line was kindly provided by Olivier Pourquié, the

Achilles-Hes7 by Ryoichiro Kageyama and the Achilles construct by Atsushi Miyawaki (Riken Center for Brain Science). P.S. was supported by KWF grant 13661 from the Dutch Cancer Foundation. This work was supported by the Hubrecht Institute and received funding from the European Research Council under an ERC starting grant agreement no. 850554 to K.F.S. In addition, this research was supported in part by grant NSF PHY-1748958 to the Kavli Institute for Theoretical Physics (KITP).

Author contributions

Conceptualization: Y.A., P.S. and K.F.S., Methodology: Y.A., Software: P.S., Formal Analysis: P.S., Y.A. and K.F.S., Investigation: Y.A., M.J.O, W.T. and K.F.S., Resources: W.T. and W.H.M.M., Writing – Original draft: Y.A. and K.F.S., Writing – Review and Editing: Y.A., K.F.S., M.B., Supervision, Project Administration and Funding acquisition: K.F.S.

Declaration of interests

The authors declare no competing interests.

Figure legends

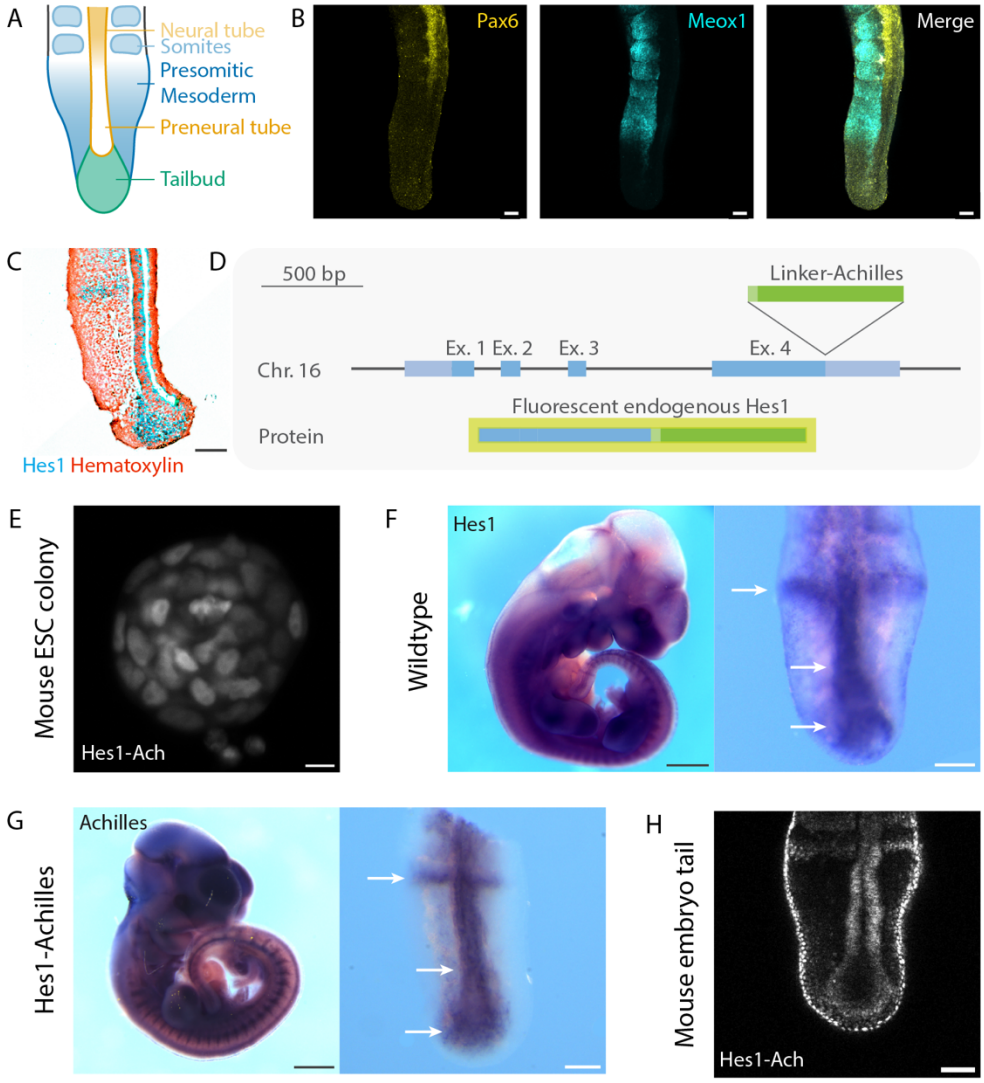

Figure 1. Generation of a Hes1-Achilles mouse line to study Hes dynamics in the posterior embryonic tail. A Schematic representation of the posterior mouse embryonic tail. Tailbud (green) differentiate into PSM (blue), which gives rise to somites (light blue), and the pre-NT (yellow), which differentiates into the NT (light yellow). **B** Representative image of a E10.5 embryonic tail stained by HCR for the mesodermal marker Meox1 and neural marker Pax6. Scale bar is 100 µm. **C** 5 µm section of an ISH of an E10.5 embryonic tail for Hes1 (as shown in Fig. S1F). Scale bar is 100 µm. **D** Schematic representation of the tagging strategy for the Hes1-Achilles mouse line. Hes1 was endogenously tagged with linker-Achilles. **E** Representative image of a mouse ESC colony expressing the Hes1-Achilles construct. Note the variable expression in the different cell types. Scale bar is 10 µm. **F, G** Representative images of ISH of an E10.5 embryo for Hes1 (**F**) (as shown in Fig. S1F) and Achilles (**G**). Right panel shows magnification of the posterior embryonic tail. Arrows highlight the expression

446 pattern in the posterior embryonic tail. Scale bar is 100 μm. **H** Representative image of an
447 E10.5 embryonic tail expressing the Hes1-Achilles reporter. Scale bar is 100 μm.

448

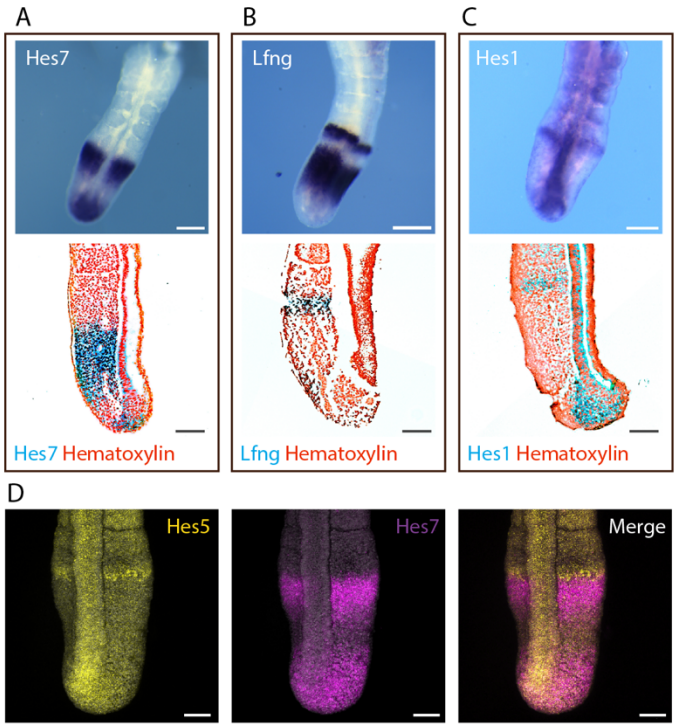

Figure S1. Hes1 and Hes5 are expressed in the pre-NT and tailbud region of the E10.5 embryo. Visualization of mRNA levels in E10.5 embryonic tails by ISH (**A-C**) and HCR (**D**). **A-C** ISH of Hes7 (**A**), Lfng (**B**) and Hes1 (**C**) (**C** as shown in Fig. 1C, F). Upper panel shows representative image of whole embryonic tail, lower panel 5 µm section counterstained with Hematoxylin. Note the high expression levels of Hes1 in the pre-NT. **D** Expression of target genes Hes5 and Hes7 in embryonic tails visualized by HCR. Scale bar is 100 µm.

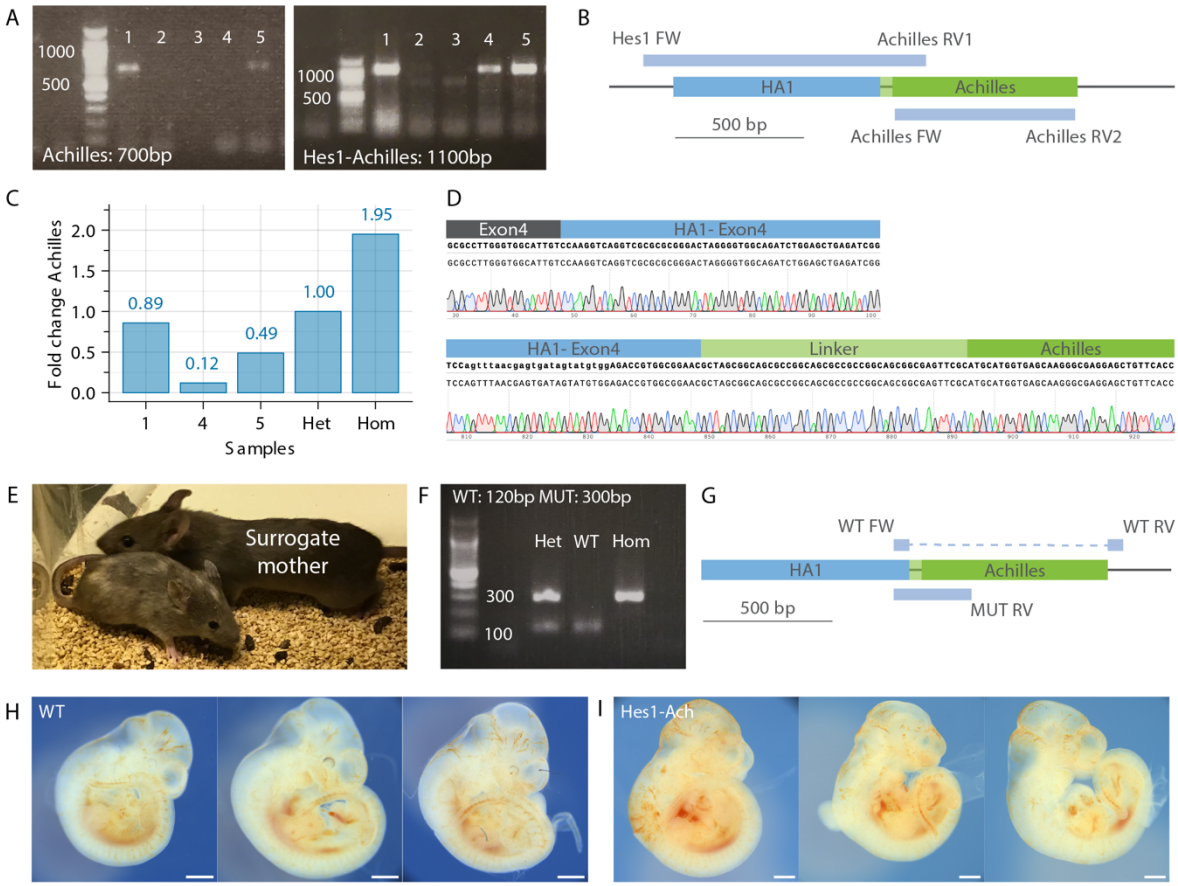

Figure S2. Characterization of Hes1-Achilles reporter mouse line. A, B Genotyping for positive clones using primers (forward (FW) and reverse (RV)) against Achilles and against a product that crosses the homology arm (HA). In **A** a representative gel and in **B** a scheme of the expected gene locus are shown. **C** Integration of exactly one copy of Achilles was confirmed by qPCR (heterozygous (Het) and homozygous (Hom)). **D** Example of sequencing result of a correctly integrated clone. **E** Chimeric mice were generated by blastocyst injection. **F, G** Genotyping of positive mice is performed using primers to detect integration wildtype (WT) and mutated alleles. In **F** representative gels and in **G** a scheme of the expected gene locus are shown. **H, I** Representative images of E10.5 wildtype (WT) (**H**) and Hes1-Achilles homozygous embryos (**I**) are represented. Scale bar is 500 µm.

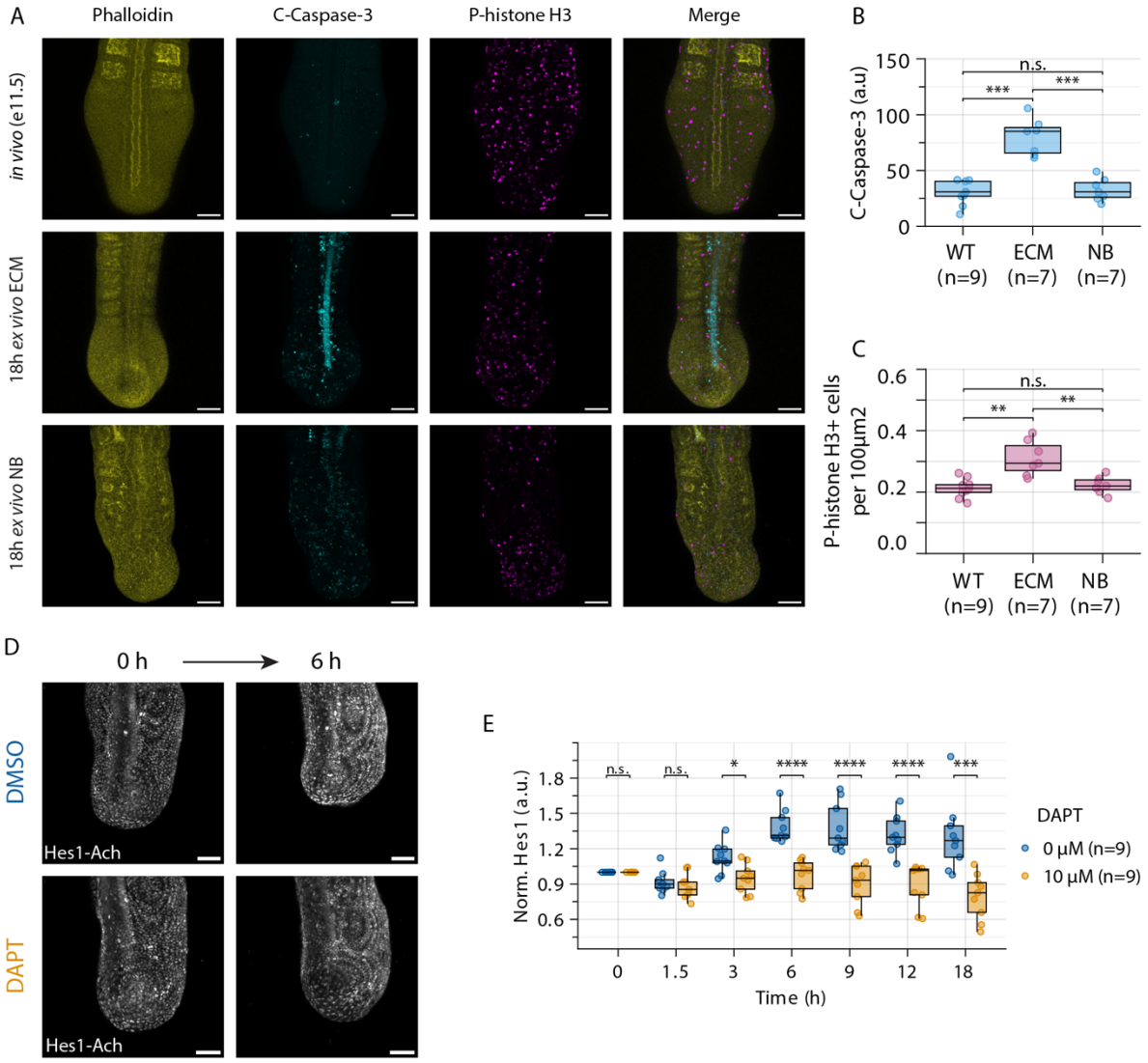

Figure 2. Inhibition of Notch signalling results in a decrease in Hes1-Achilles levels in *ex vivo* cultured E10.5 embryonic tails. A-C Comparison of different culture media to optimize for the survival of the pre-NT *ex vivo*. Embryonic tails were cultured *ex vivo* for 18 h in embryo culture medium (ECM) or neurobasal (NB) medium and compared to uncultured (*in vivo*) E11.5 embryos. Immunostaining against cleaved-caspase 3 (C-Caspase 3, apoptosis) phospho-histone H3 (P-histone H3, mitosis) and counterstaining with Phalloidin was performed. In **A** representative images are shown. In **B** the intensity of cleaved caspase 3 signal in the embryonic tail and in **C** the number of mitotic cells in the pre-NT were quantified. **D, E** E10.5 embryonic tails were cultured *ex vivo* and incubated with DMSO control or the gamma-secretase inhibitor DAPT. Hes1-Achilles intensity was measured over time. In **D** representative images and in **E** the quantification of Hes1-Achilles intensity in the embryonic tail are shown. Scale bar is 100 µm. Dots in boxplots represent individual data points. * is $p<0.05$, ** is $p<0.01$, *** is $p<0.001$, **** is $p<0.0001$.

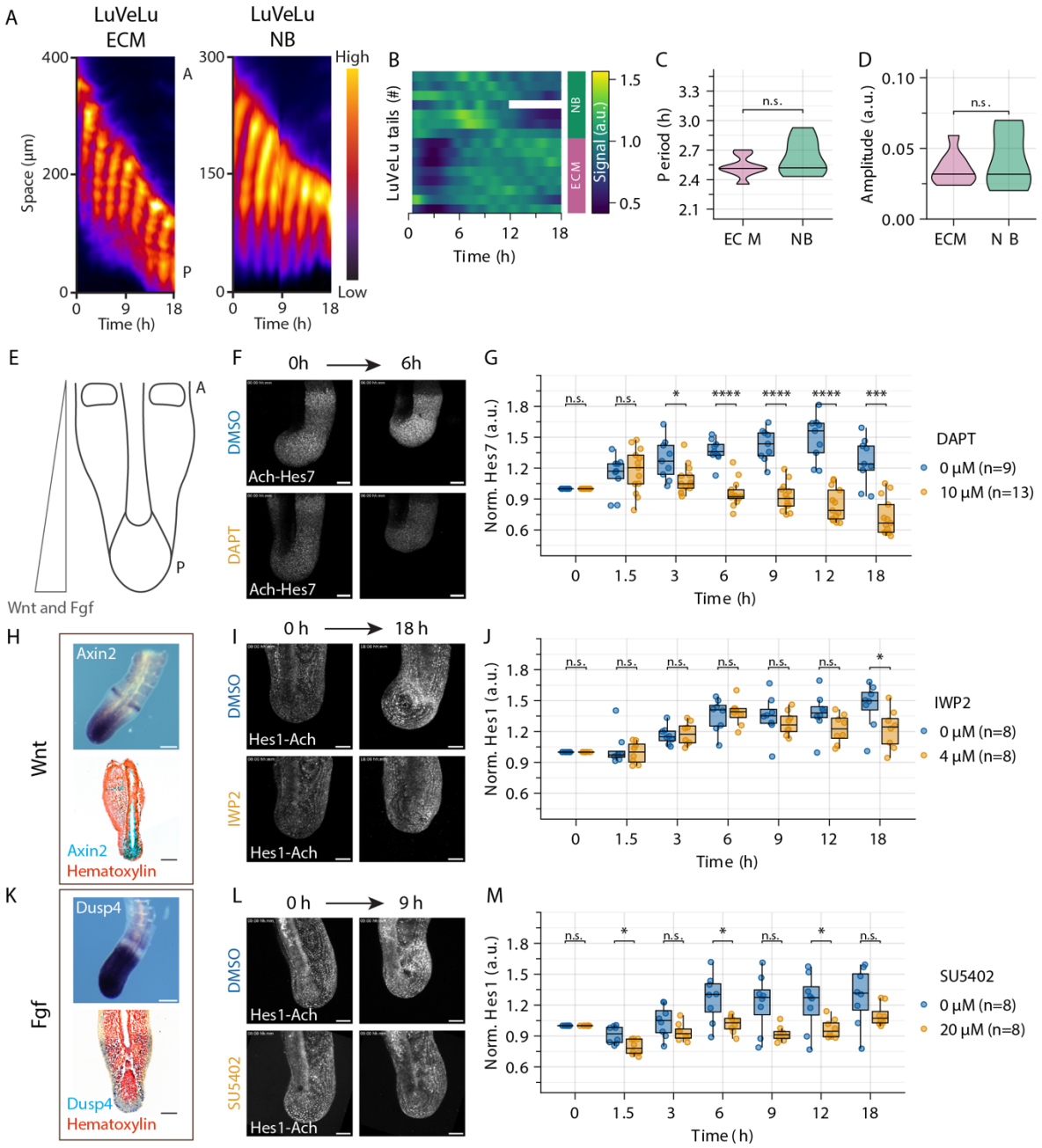

483

484 **Figure S3. Differential effect of signalling perturbation on *ex vivo* cultured E10.5**
485 **embryonic tails. A-D** Embryonic tails were cultured *ex vivo* in either ECM or NB medium.
486 Intensity of the dynamic signalling reporters LuVeLu was measured. **A** Kymographs generated
487 along the PSM from the posterior (P) to the anterior (A) of a growing embryonic tail cultured
488 in ECM (left panel) or NB medium (right panel) were generated. Note the wave dynamics
489 visible in both. **B** Heatmap of samples illustrating signalling dynamics in the different culture
490 conditions using LuVeLu as reporter line. **C, D** Quantification of period (**C**) and amplitude (**D**)
491 of the signalling dynamics shown in **B**. ECM n=8 tails, NB n=7 tails **E-M** Effect of signalling
492 inhibition on *ex vivo* cultured embryonic tails. **E** Schematic representation of embryonic tail
493 highlighting the gradients of Wnt and FGF along the tissue. **F, G** E10.5 embryonic tails were

494 cultured *ex vivo* and incubated with DMSO control or the gamma-secretase inhibitor DAPT.
495 Achilles-Hes7 intensity was measured over time. In **F** representative images and in **G** the
496 quantification of Hes1-Achilles intensity in the embryonic tail are shown. **H** ISH of E10.5
497 embryonic tail for Wnt target gene Axin2. Upper panel shows representative image of whole
498 embryonic tail, lower panel a 5 µm section counterstained with Hematoxylin. **I, J** E10.5
499 embryonic tails were cultured *ex vivo* and incubated with DMSO control or the porcupine
500 inhibitor IWP2. Hes1-Achilles intensity was measured over time. In **I** representative images
501 and in **J** the quantification of Hes1-Achilles intensity in the embryonic tail are shown. **K** ISH of
502 E10.5 embryonic tail for FGF target gene Dusp4. Upper panel shows representative image of
503 whole embryonic tail, lower panel a 5 µm section counterstained with Hematoxylin. **L, M** E10.5
504 embryonic tails were cultured *ex vivo* and incubated with DMSO control or the FGF receptor
505 inhibitor SU5402. Hes1-Achilles intensity was measured over time. In **L** representative images
506 and in **M** the quantification of Hes1-Achilles intensity in the embryonic tail are shown. Scale
507 bar is 100 µm. Dots in boxplots represent individual data points. * is $p<0.05$, ** is $p<0.01$, ***
508 is $p<0.001$, **** is $p<0.0001$.

509

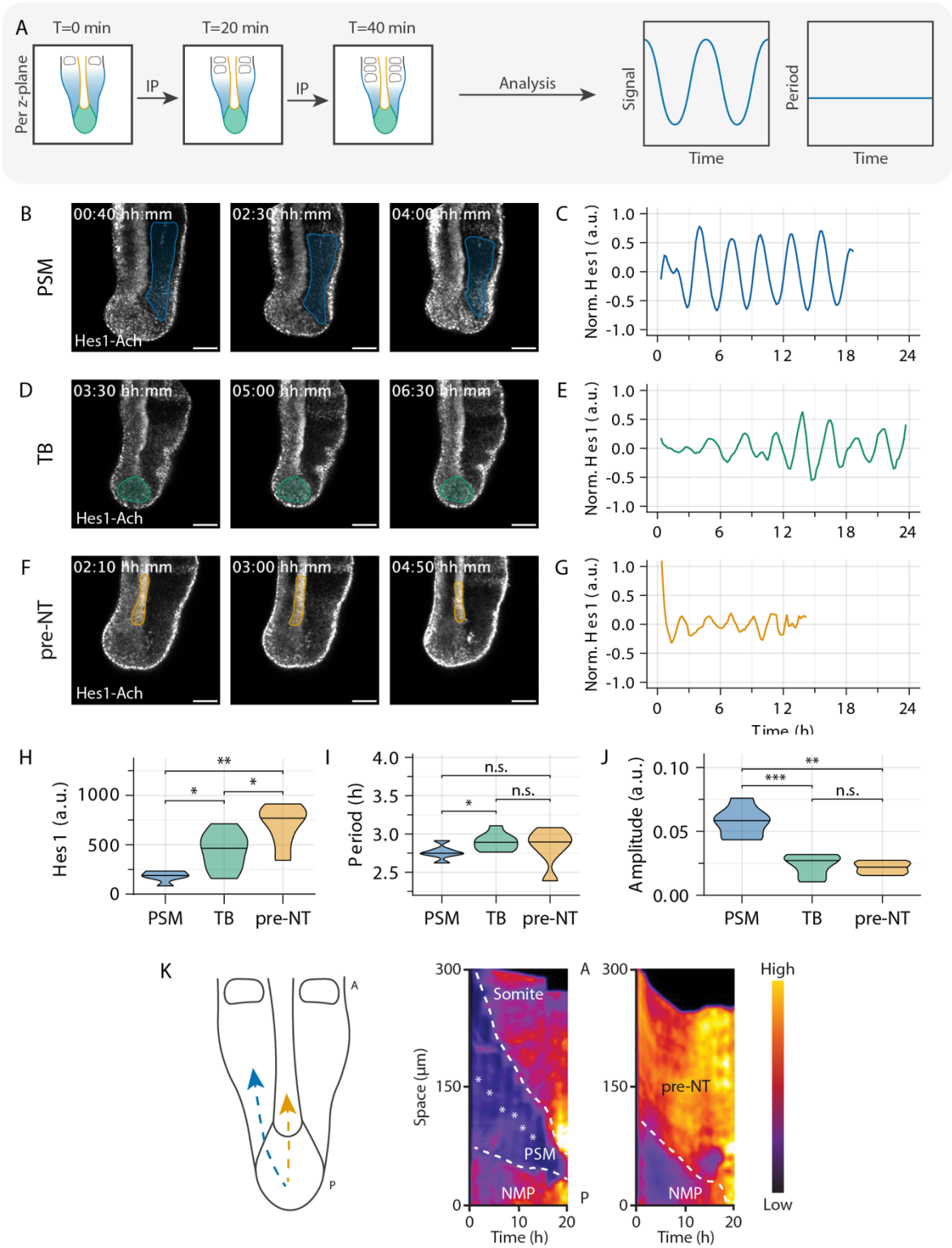

Figure 3. Pre-NT and tailbud region in *ex vivo* cultured E10.5 embryonic tails show low amplitude oscillations at population level. A Embryonic tails were cultured *ex vivo* and Hes1-Achilles intensity measured by fluorescence real-time imaging (corresponding to correctly positioned control samples from Figure 2 and S3). Regions of interest were selected manually and interpolated (IP) between timepoints. Hes1-Achilles dynamics were then

quantified by wavelet transform. **B, C** Quantification of Hes1-Achilles dynamics in the PSM region. Representative snapshots are shown in **B** and the corresponding timeseries data (mean-normalised) of single PSM region (as indicated in **B**) is shown in **C**. **D, E** Quantification of Hes1-Achilles dynamics in the TB region. Representative snapshots are shown in **D** and the corresponding timeseries data (mean-normalised) of single TB region (as indicated in **D**) is shown in in **E**. **F, G** Quantification of Hes1-Achilles dynamics in the pre-NT region. Representative snapshots are shown in **F** and the corresponding timeseries data (mean-normalised) of single pre-NT region (as indicated in **F**) is shown in in **G**. **H** Quantification of absolute Hes1-Achilles intensity in the different regions (PSM (n=6 tails), TB (n=8 tails) and pre-NT (n=6 tails)). **I, J** Quantification of the period (**I**) and amplitude (**J**) by wavelet transform. **K** Left panel: kymographs of Hes1-Achilles dynamics were generated along the arrows indicated (PSM in blue and pre-NT in yellow) from the posterior (P) to the anterior (A) region of the embryonic tail. Right panel: Representative kymographs for PSM and pre-NT are shown. Hes1-Achilles wave is indicated by asterisk. Scale bar is 100 μm. * is $p<0.05$, ** is $p<0.01$, *** is $p<0.001$, **** is $p<0.0001$.

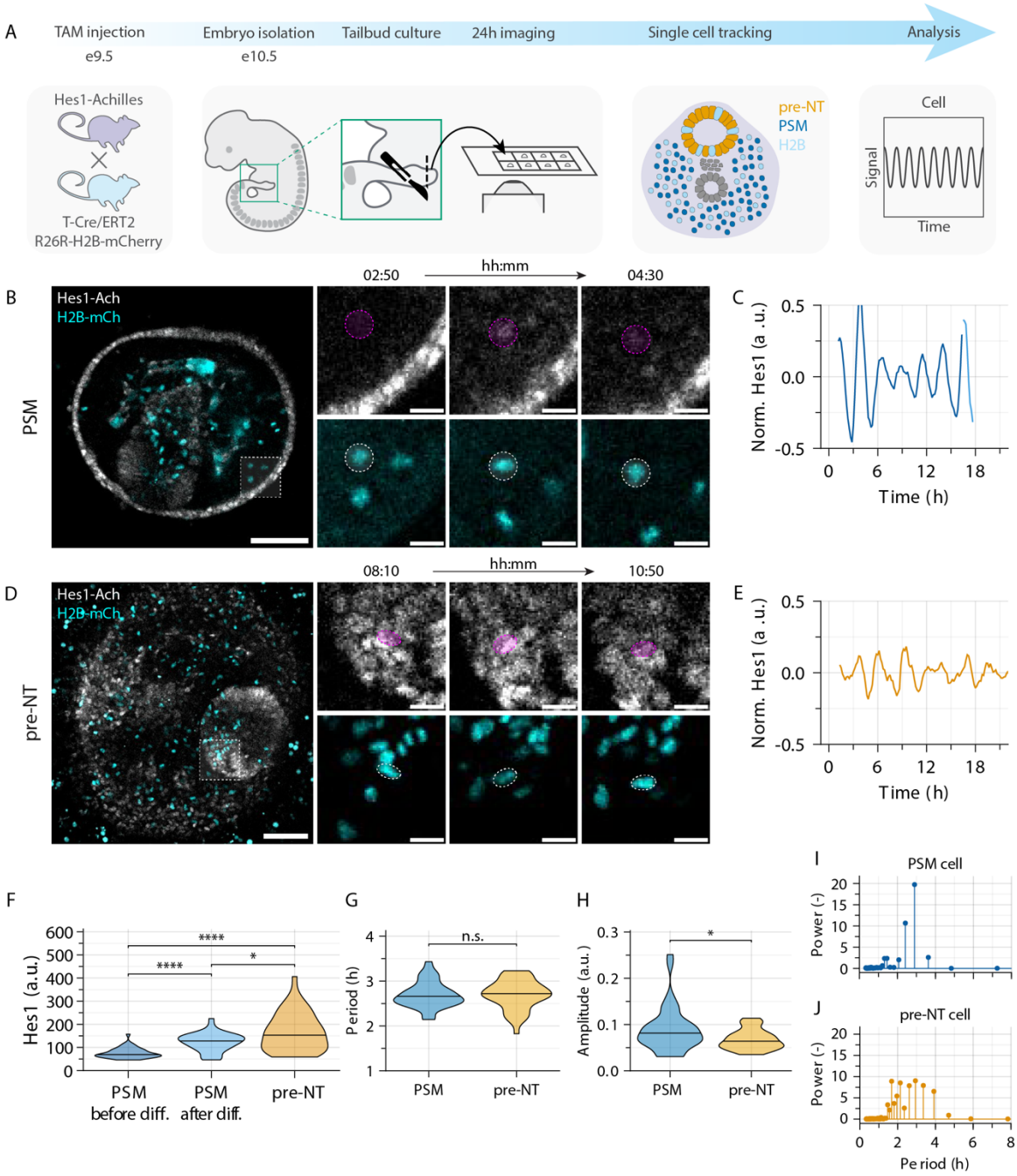

Figure 4. Both PSM and pre-NT cells show Hes1 oscillations at single-cell level. A Sparse labelling with H2B-mCherry was induced by injection of 1 mg Tamoxifen (TAM). Embryonic tail tips were cultured *ex vivo* on fibronectin-coated dishes. Hes1-Achilles and H2B-mCherry intensity were measured by fluorescence real-time imaging. Single cells were tracked semi-automatically to quantify Hes1-Achilles dynamics. **B, C** Quantification of Hes1-Achilles dynamics in PSM cells. Representative snapshots are shown in **B**. Representative timeseries data (mean-normalised) of a single PSM cell (blue) is shown in **C**. Differentiated PSM cell is indicated by light blue colour. **D, E** Quantification of Hes1-Achilles dynamics in pre-NT cells. Representative snapshots are shown in **D**. Representative timeseries data

542 (mean-normalised) of single pre-NT cell is shown in **E**. **F** Quantification of absolute Hes1-
543 Achilles intensity in the different regions (diff. = differentiation) of the embryonic tail. **G, H**
544 Quantification of the period (**G**) and amplitude (**H**) by wavelet transform. **I, J** Representative
545 Fourier spectrum of a single PSM or pre-NT cell are shown. Note that there is one dominant
546 peak at 2.5 h for PSM, but not one dominant peak for pre-NT. Scale bar is 100 µm. * is $p<0.05$,
547 ** is $p<0.01$, *** is $p<0.001$, **** is $p<0.0001$. PSM cells: n=39; pre-NT cells: n=40.

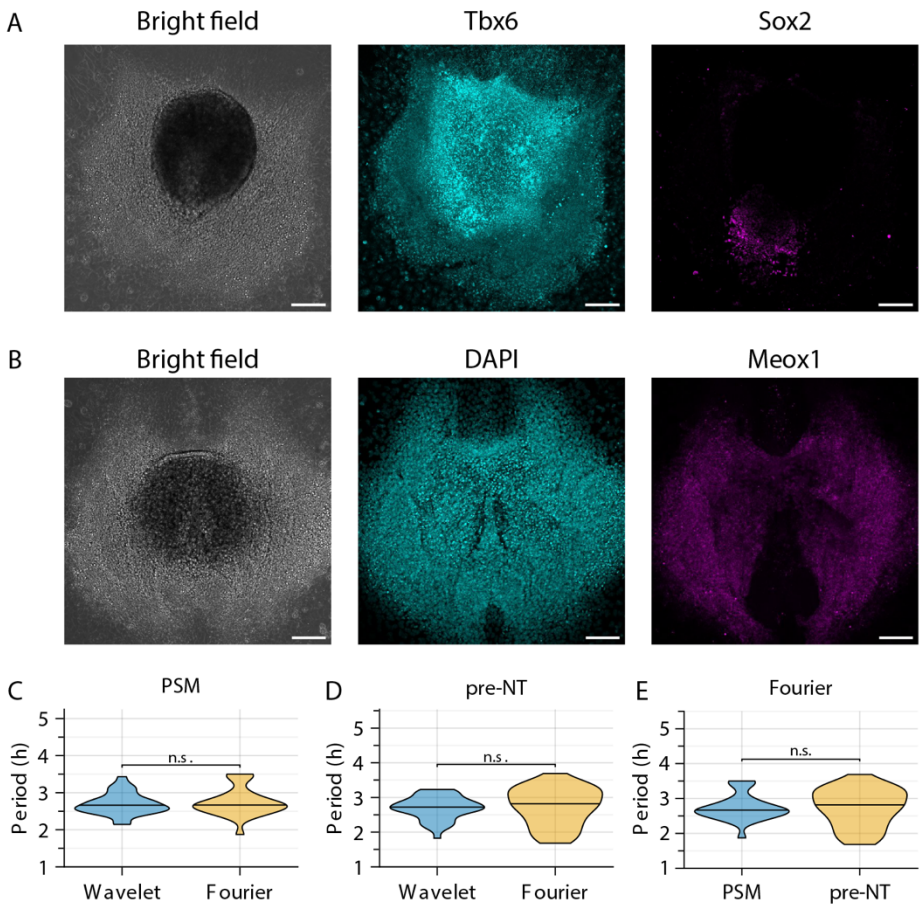

Figure S4. Characterization of 2D *ex vivo* cultures of E10.5 embryonic tail tips. A, B Cultures were fixed after 18 h and stained. **A** Representative image of immunostaining for PSM marker Tbx6 and neural marker Sox2. **B** Representative image of HCR for Meox1 and counterstaining for nuclei (DAPI). Scale bar is 100 µm. **C, D** Periods were quantified using wavelet transform or Fourier transform for PSM cells (**C**) or pre-NT cells (**D**). In **E** periods were quantified using Fourier transform for PSM cells and pre-NT cells. The coefficient of variation is 0.1 for PSM cells and 0.2 for pre-NT cells. * is $p<0.05$, ** is $p<0.01$, *** is $p<0.001$, **** is $p<0.0001$. PSM cells: n=39; pre-NT cells: n=40.

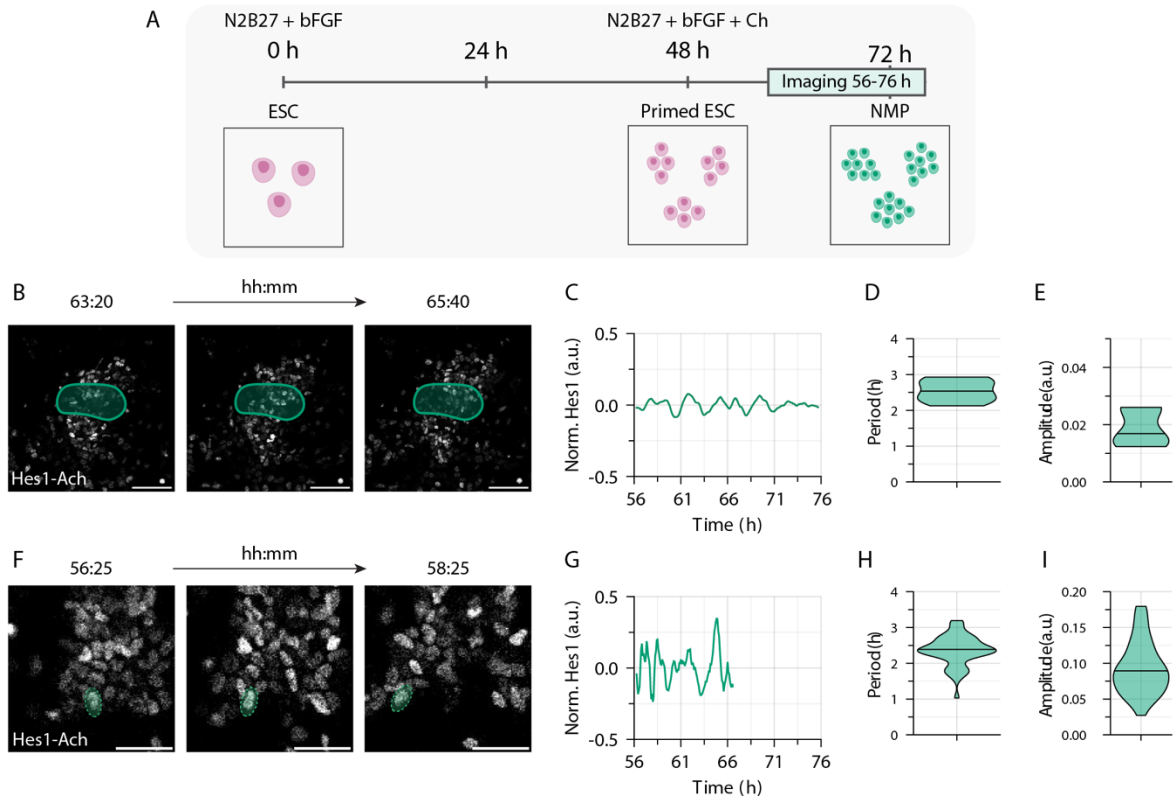

Figure 5. Hes1 shows noisy oscillations in *in vitro* differentiated NMPs. A Mouse ESCs were differentiated *in vitro* to NMPs. Hes1-Achilles intensity was measured by fluorescence real-time imaging from 56 - 76 h of differentiation. **B-E** Quantification of Hes1-Achilles dynamics in whole NMP colonies (n=8). Representative snapshots are shown in **B**. Timeseries data (mean-normalised) of representative NMP colony is shown in **C**. **D, E** Quantification of the period (**D**) and amplitude (**E**) by wavelet transform. Scale bar 100 µm. **F-I** Quantification of Hes1-Achilles dynamics in single NMP cells (n=46). Single cells were tracked manually to quantify Hes1-Achilles dynamics. Representative snapshots are shown in **F**. Representative timeseries data (mean-normalised) of NMP cells is shown in **G**. **H, I** Quantification of the period (**H**) and amplitude (**I**) by wavelet transform. Scale bar 50 µm. Note that data for control corresponds to control data in Figure S5.

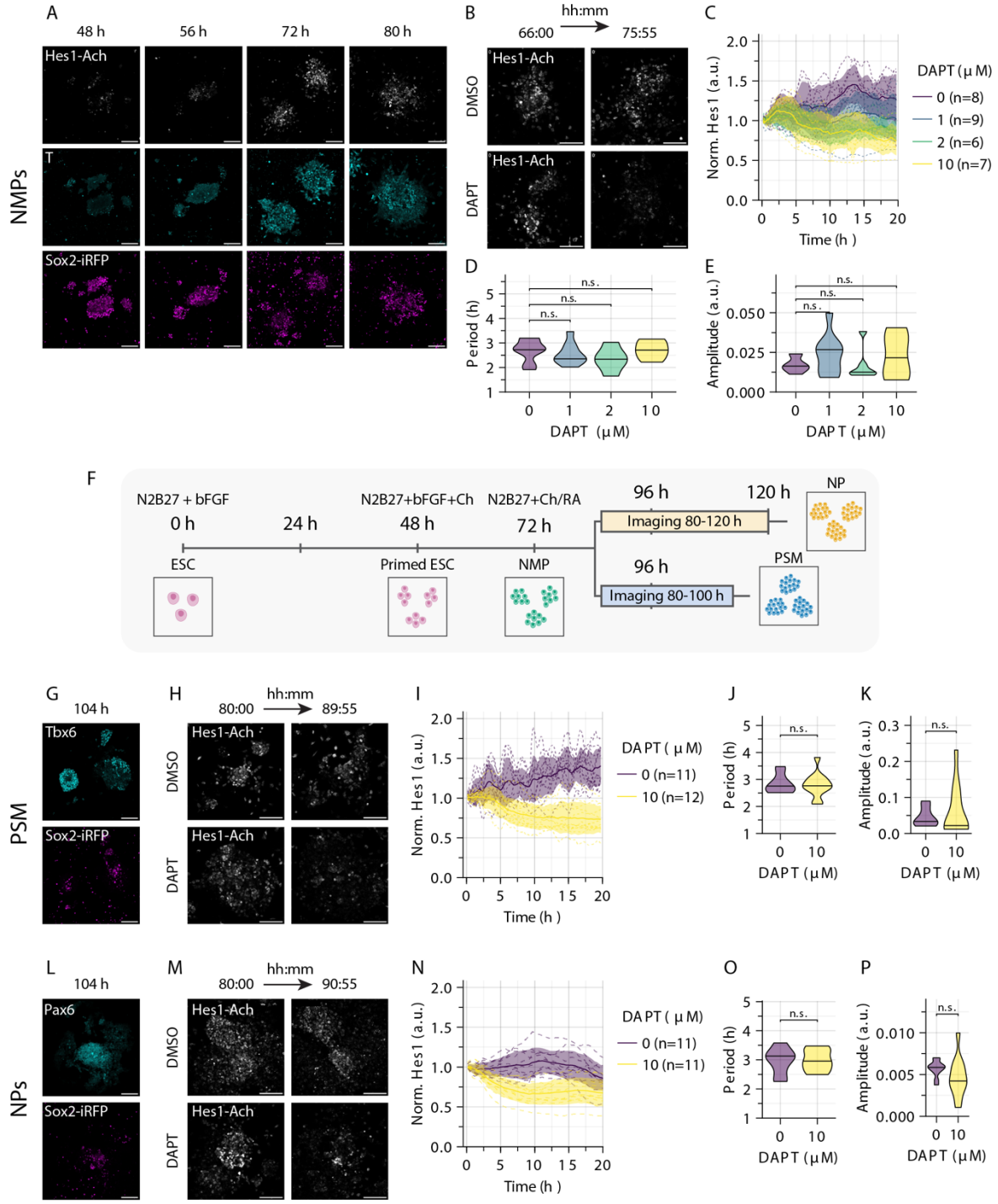

Figure S5. Population-wide Hes1 dynamics in *in vitro* differentiated cells. A Mouse ESCs expressing Hes1-Achilles and Sox2-iRFP were differentiated *in vitro* to NMPs. Cells were fixed at the indicated timepoints and immunostaining against T was performed. Representative images are shown. **B-E** Quantification of Hes1-Achilles dynamics in whole colonies. Representative snapshots are shown in **B**. *In vitro* differentiated NMPs were incubated with DMSO control or the gamma-secretase inhibitor DAPT. Hes1-Achilles intensity was measured over time. In **C** individual tracks (dotted lines), mean (solid line) and standard deviation (area)

of the timeseries data (DMSO-normalised) are shown. Note the dose-dependent decrease in Hes1-Achilles intensity. Quantification of the period (**D**) and amplitude (**E**) by wavelet transform. **F-K** Hes1-Achilles dynamics in *in vitro* differentiated PSM colonies. **F** Mouse ESCs expressing Hes1-Achilles and Sox2-iRFP were differentiated *in vitro* along NMPs to PSM or neural progenitor (NP) colonies. Hes1-Achilles intensity was measured by fluorescence real-time imaging from 80 - 100 h of differentiation for PSM colonies and 80 – 120 h of differentiation for NP colonies. **G** Colonies were fixed at the indicated timepoints and immunostaining against Tbx6 was performed. Representative images are shown. **H-K** Quantification of Hes1-Achilles dynamics in PSM colonies. Representative snapshots are shown in **H**. *In vitro* differentiated PSM colonies were incubated with DMSO control or the gamma-secretase inhibitor DAPT. Hes1-Achilles intensity was measured over time. In **I** individual tracks (dotted lines), mean (solid line) and standard deviation (area) of the timeseries data (DMSO-normalised) are shown. Quantification of the period (**J**) and amplitude (**K**) by wavelet transform. **L** Cells were fixed at the indicated timepoints and immunostaining against Pax6 was performed. Representative images are shown. **M-P** Quantification of Hes1-Achilles dynamics in NP colonies. Representative snapshots are shown in **M**. *In vitro* differentiated NP colonies were incubated with DMSO control or the gamma-secretase inhibitor DAPT. Hes1-Achilles intensity was measured over time. In **N** individual tracks (dotted lines), mean (solid line) and standard deviation (area) of the timeseries data (DMSO-normalised) are shown. Quantification of the period (**O**) and amplitude (**P**) by wavelet transform. Scale bar is 100 μm. Note that data for control corresponds to control data in Figure 5.

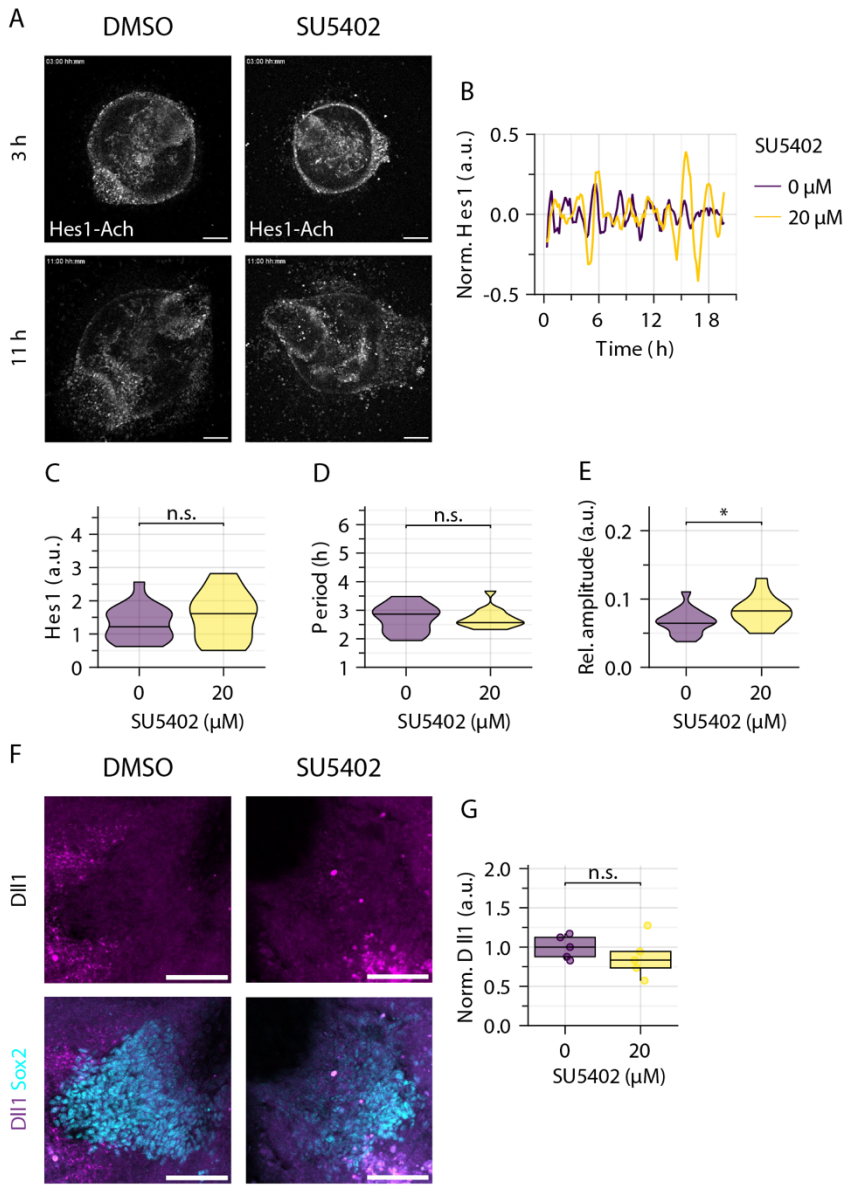

Figure 6. Induced differentiation by FGF inhibition leads to Hes1 dynamics with increased amplitude. Embryonic tail tips were cultured with DMSO control or the FGF receptor inhibitor SU5402. **A** Representative snapshots of the timeseries are shown. Scale bar is 100 μm. **B** Representative timeseries data is shown. **C-E** Quantification of absolute (DMSO-normalised) Hes1-Achilles expression levels (**C**), period (**D**) and relative (mean-normalised) amplitude (**E**) by wavelet transform (0 μM n=15, 20 μM n=15). Further analysis shown in Figure S6. **F, G** Cultures were fixed after 21 h and immunostaining against Dll1 and Sox2 was performed. Representative images are shown in **F** and the quantification in **G** (0 μM n=5, 20 μM n=5). Scale bar is 50 μm. * is p<0.05, ** is p<0.01, *** is p<0.001, **** is p<0.0001.

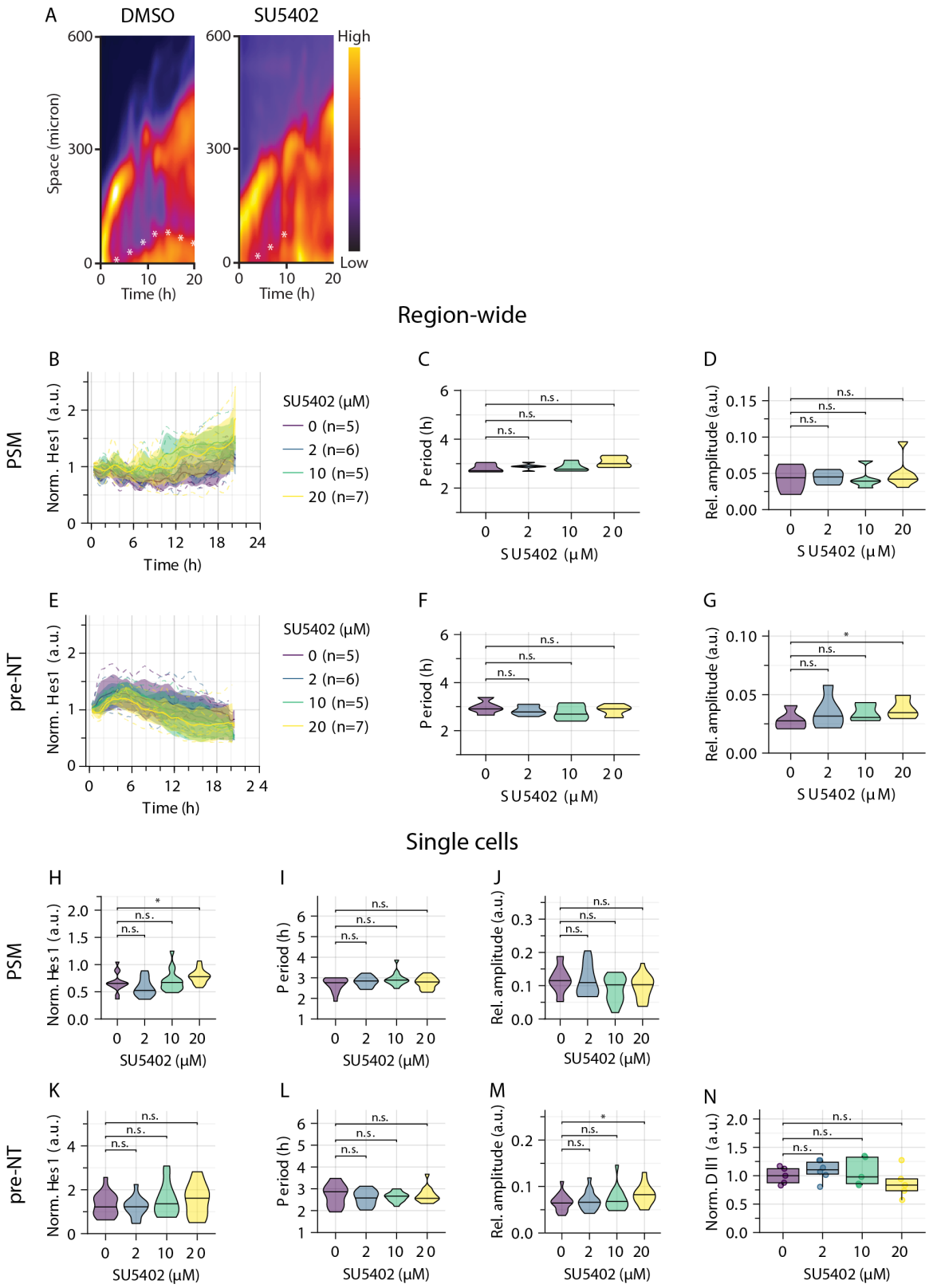

611

612 **Figure S6. FGF inhibition leads to an increase in Hes1 oscillation amplitude in pre-NT**
613 **cells.** Further analysis of data shown in Figure 6. **A** Representative kymographs for PSM
614 region upon DMSO and FGF inhibition (SU5402) are shown. Hes1-Achilles wave is indicated

by asterisk. **B-D** Quantification of population-wide dynamics in the PSM and pre-NT regions. **B** individual tracks (dotted lines), mean (solid line) and standard deviation (area) of the timeseries data (normalised to t=0 h of DMSO) are shown. **C, D** Quantification of period (**C**) and relative (mean-normalized) amplitude (**D**) by wavelet transform. **E-G** Quantification of Hes1-Achilles dynamics in pre-NT region. **E** individual tracks (dotted lines), mean (solid line) and standard deviation (area) of the timeseries data (DMSO-normalised) are shown. **F, G** Quantification of period (**F**) and relative (mean-normalized) amplitude (**G**) by wavelet transform. **H-J** Quantification of Hes1-Achilles dynamics in PSM cells. Quantification of absolute (normalised to t=0 h of DMSO) Hes1-Achilles expression levels (**H**) and period (**I**) and relative (mean-normalised) amplitude (**J**) by wavelet transform (0-10 μM: n=15; 20 μM: n=18). **K-M** Quantification of Hes1-Achilles dynamics in pre-NT cells. Quantification of absolute (DMSO-normalised) Hes1-Achilles expression levels (**K**) and period (**L**) and relative (mean-normalised) amplitude (**M**) by wavelet transform. **N** Cultures were fixed after 18 h and immunostaining against Dll1 and Sox2 was performed. Quantification of Dll1 in the Sox2-positive region is depicted (per concentration minimal n=5).

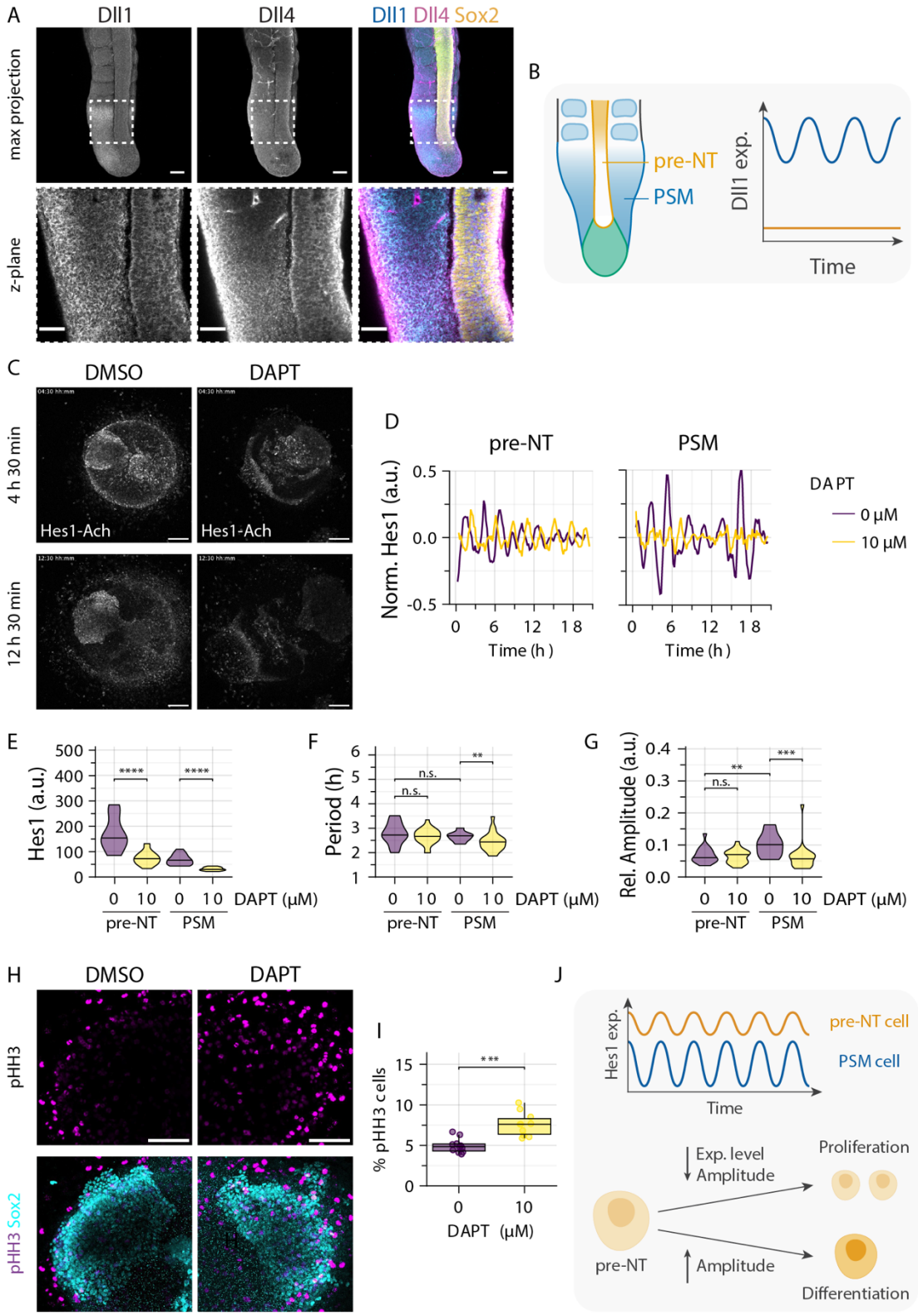

Figure 7. Notch inhibition has a differential effect on Hes1 oscillations in PSM and pre-NT cells. A Representative image of immunostaining of an E10.5 embryonic tail for Dll1, Dll4 and the neural marker Sox2. Scale bar of top panel is 100 μm and bottom panel is 50 μm. **B** Schematic illustrating that Dll1 oscillates at high levels in the PSM[11], whereas Dll1 levels are

low and non-oscillatory in the pre-NT. **C-I** Embryonic tail tips were cultured with DMSO control or the gamma-secretase inhibitor DAPT. **C** Representative snapshots of the timeseries are shown. Scale bar is 100 μm. **D** Representative timeseries data for pre-NT cells (left panel) and PSM cells (right panel) cells are shown. **E-G** Quantification of absolute Hes1-Achilles expression levels (**E**), period (**F**) and relative (mean-normalised) amplitude (**G**) by wavelet transform. (0 μM n=18, 10 μM n=21). Further quantification shown in Figure S7. **H, I** Cultures were fixed after 18h and immunostaining against phosphorylated histone H3 (pHH3) and Sox2 was performed. Representative images are shown in **H** and the quantification of pHH3-positive cells in the Sox2-positive region in **I** (0 μM n=11, 10 μM n=10). Scale bar is 50 μm. **J** Schematic summarising lower Hes1-Achilles expression level and higher Hes1-Achilles amplitude in PSM cells compared to pre-NT. In addition, decreased Hes1-Achilles expression level and amplitude led to proliferation of pre-NT cells, while increased Hes1-Achilles amplitude correlates with differentiation.

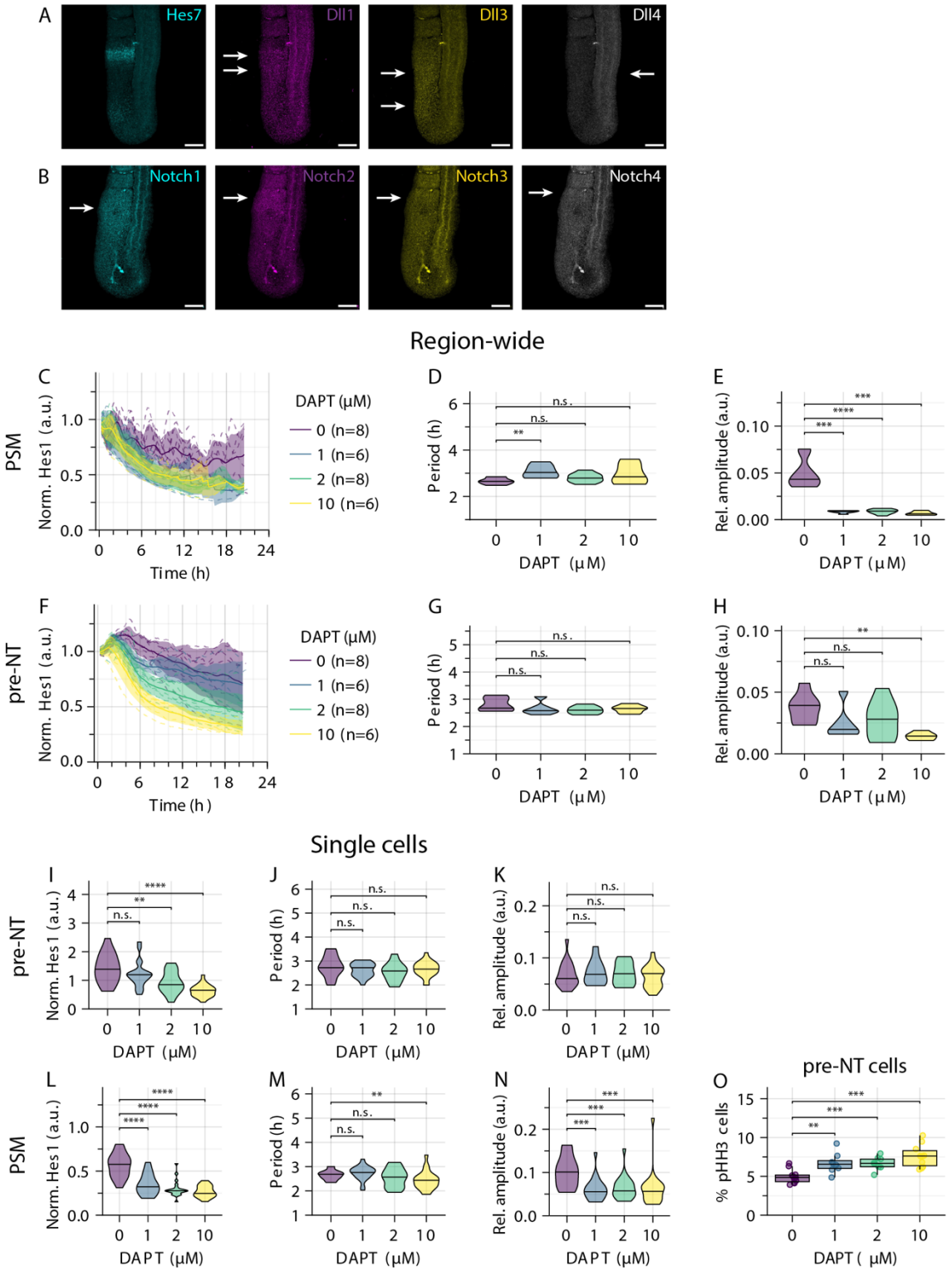

Figure S7. Notch inhibition has different effects on Hes1 dynamics in the pre-NT and PSM. A, B Expression of Delta-like ligands in comparison to Hes7 (**A**) and expression of Notch receptors (**B**) was visualized in E10.5 embryonic tails by HCR. Arrows highlight the expression pattern in the posterior embryonic tail. **C-O** Further quantification of the data shown in Figure 7. E10.5 embryonic tails were cultured *ex vivo* as 2D cultures and treated with the indicated

concentrations of the Notch inhibitor DAPT. **C-E** Quantification of population-wide dynamics in the PSM region. **C** individual tracks (dotted lines), mean (solid line) and standard deviation (area) of the timeseries data (normalised to t=0 h of DMSO) are shown. **D, E** Quantification of period (**D**) and relative (mean-normalized) amplitude (**E**) by wavelet transform. **F-H** Quantification of population-wide dynamics in the pre-NT region. **F** individual tracks (dotted lines), mean (solid line) and standard deviation (area) of the timeseries data (normalised to t=0 h of DMSO) are shown. **G, H** Quantification of period (**G**) and relative (mean-normalized) amplitude (**H**) by wavelet transform. **I-K** Quantification of Hes1-Achilles dynamics in single pre-NT cells. Quantification of absolute (DMSO-normalised) Hes1-Achilles expression levels (**I**) and period (**J**) and relative (mean-normalised) amplitude (**K**) by wavelet transform (0 μM: n=18; 1 μM: n=16; 2 μM: n=21; 10 μM: n=21). **L-N** Quantification of Hes1-Achilles dynamics in single PSM cells. Quantification of absolute (DMSO-normalised) Hes1-Achilles expression levels (**L**) and period (**M**) and relative (mean-normalised) amplitude (**N**) by wavelet transform (0 μM: n=18; 1 μM: n=21; 2 μM: n=21; 10 μM: n=21). **O** Cultures were fixed after 18 h and immunostaining against phosphorylated histone H3 (pHH3) and Sox2 was performed. Quantification of pHH3-positive cells in the Sox2-positive region is depicted (per concentration minimal n=8).

674 **Star Methods**

675 **Contact for reagent and resource sharing**

676 Further information and requests for resources, data or code should be addressed to the Lead
677 Contact, Katharina Sonnen (k.sonnen@hubrecht.eu).

678

679 **Experimental model and subject details**

680 **Mouse lines**

681 All animals were housed and bred according to institutional guidelines, and procedures were
682 performed in compliance with Standards for Care and Use of Laboratory Animals with approval
683 from the Hubrecht Institute ethical review board. All animal experiments were approved by the
684 Animal Experimentation Committee (DEC) of the Royal Netherlands Academy of Arts and
685 Sciences.

686 The Hes1-Achilles knock-in reporter line was generated employing standard gene targeting
687 techniques using IB10 ESCs. To generate Hes1-Achilles alleles, we targeted the stop codon
688 of the endogenous Hes1 locus with a reporter cassette coding for a linked fluorophore (Hes1-
689 linker-Achilles). The reporter cassette is linked to the Hes1 gene via a flexible GSAGS
690 sequence and includes a selection cassette. After generation of the knock-in reporter line, the
691 selection cassette was removed by Cre-mediated excision to yield the final Hes1-Achilles
692 allele, using the PGK-Cre mouse line[77].

693 The LuVeLu[46] and Achilles-Hes7[38] line were published previously. The R26R-H2B-mCherry[78]
694 ("H2B-mCherry") line (http://www.clst.riken.jp/arg/reporter_mice.html) was obtained from the
695 Riken Center for Biosystems Dynamics Research (accession number CDB0204K). The Tg(T-
696 cre/ERT2)1Lwd/J[79] ("T-Cre/ERT2") line was obtained from the Jackson Laboratory (accession
697 number #025520). The Tg(Pgk1-cre)1Lni/CrsJ[77] ("PGK-Cre") line was obtained from the
698 Jackson Laboratory (accession number #020811). The R26-CreERT2[80] ("RosaCreERT") line
699 was obtained from the Jackson Laboratory (accession number #00846).

700

701 **Cell lines**

702 For the generation of Hes1-Achilles_RosaCreERT ESCs, E3.5 blastocysts were isolated from
703 pregnant Hes1-Achilles_RosaCreERT females. Each blastocyst was transferred to a single
704 well of a 24-well plate seeded with feeder MEFs. After 6 days, cells were trypsinized and
705 expanded into a 12-well plate with feeders. Four days later, cells were expanded into 6-well

706 plates, and simultaneously used for extraction of genomic DNA followed by polymerase chain
707 reaction (PCR) to determine the genotype. After confirmation of genotype, cells were further
708 expanded for one more passage prior to freezing down. ESCs were cultured in N2B27-2i
709 medium as previously described[81].

710 The Sox2-H2B-iRFP ("Sox2-iRFP") knock-in reporter line was generated employing
711 CRISPaint[49] gene targeting techniques using Lipofectamine 3000 (ThermoFisher, L3000001)
712 and Hes1-Achilles_RosaCreERT ESCs. To generate Sox2-iRFP alleles, we targeted a PAM
713 site before the stop codon of the endogenous Sox2 locus with a reporter cassette coding for
714 a separated H2B gene linked to a fluorophore (Sox2-T2A-H2B-linker-iRFP). The reporter
715 cassette is separated from the Sox2 gene via a small 2A sequence. Furthermore, the
716 fluorophore is linked to the H2B gene via a flexible GSAGS sequence. The selection cassette
717 is also separated from the reporter cassette via a small 2A sequence. Selection occurred two
718 days after transfection and lasted three days. Colonies were picked and transferred to a single
719 well of a 96-well plate seeded with irradiated feeder MEFs. Colonies were then expanded,
720 genotyped and frozen as explained above.

721

722 **Methods details**

723 **Transgenic, mouse strains and animal work**

724 For all experiments (unless stated otherwise) female mice were sacrificed on 10.5 dpc and
725 embryos dissected. Dissections were performed in PBS supplemented with 1 % Bovine Serum
726 Albumin (Biowest, P6154), 200 µg Penicillin-Streptomycin (Gibco, 15140122), 1x GlutaMAX
727 (Gibco, 35050038) and 10 % Glucose Solution 45 (Sigma-Aldrich, G8769).

728 *Ex vivo* culture was performed as described previously[45,46,68]. The neurobasal medium used
729 to culture *ex vivo* samples consists Special Advanced DMEM/F-12 (Cell Culture Technologies)
730 and Neurobasal medium (Gibco, 12348017) (1:1), 1x N2 (Gibco, 17502048), 1x B27 (Gibco,
731 12587010), 1x GlutaMAX (Gibco, 35050038), 0.004 % Bovine Serum Albumin (Biowest,
732 P6154), 0.1 mM 2-Mercaptoethanol and 200 µg Penicillin-Streptomycin (Gibco, 15140122)
733 The following small molecule inhibitors dissolved in DMSO were used at the concentration
734 indicated in the text and Figure legends: FGF-basic ("bFGF", Prepotech, 450-33), CHIR99021
735 ("Chiron", Sigma-Aldrich, SML1046), DAPT (Sigma-Aldrich, D5942), IWP-2 (Sigma-Aldrich,
736 I0536), Retinoic acid ("RA", Sigma-Aldrich, R2625-50MG), and SU5402 (Sigma-Aldrich,
737 SML0443). Samples were imaged in 8-well Chambered Coverglass w/ non-removable wells
738 (ThermoFisher, 155411PK)

739 For experiments including Hes1-Achilles mice, individual mice were genotyped by PCR using
740 primers Hes1-C-forward (GACCTCGGTGGGTCCTAACGC), linker-Achilles-reverse
741 (CTTGCCGGTGGTGCAGATCAG) and Hes1-N-reverse
742 (GAGGTGGGCTAGGGACTTTACGG).

743

744 ***In vitro* differentiation**

745 ESCs were differentiated to NMP, mesodermal or neural fate as described previously[48,50]. To
746 minimise fluorescent background, Special Advanced DMEM/F-12 (Cell Culture Technologies),
747 without phenol red was used. Every time, cells were differentiated and imaged in µ-Dish 35
748 mm Quad (Ibidi, 80416).

749

750 **Immunostaining**

751 For immunostaining, samples were fixed in 4 % formaldehyde for 30 minutes and kept in PBS
752 at 4°C. Commercial antibodies were used including anti-Dll1 rat (MABN2284, Sigma-Aldrich),
753 anti-Dll4 goat (AF1389-SP, R&D systems), anti-Cleaved Caspase-3 rabbit (9661S, CST), anti-
754 phospho Histone H3 mouse (05-806, Sigma-Aldrich), Alexa Fluor 555 Phalloidin (A34055,
755 ThermoFisher), anti-Tbx6 rabbit (ab38883, abcam), anti-Sox2 mouse (ab79351, abcam), anti-
756 Sox2 rabbit (ab92494, abcam), anti-T human/mouse (AF2085-SP, R&D systems), anti-Pax6
757 recombinant (ab195045, abcam), Goat anti-Rat Alexa Fluor 555 (A-21434, ThermoFisher),
758 Donkey anti-Rabbit Alexa Fluor 488 (A-21206, ThermoFisher), Donkey anti-Rabbit Alexa Fluor
759 568 (A10042 ThermoFisher), Donkey anti-rabbit Alexa Fluor 405 (A48258, ThermoFisher),
760 Donkey anti-mouse Alexa Fluor 647 (A-31571, ThermoFisher), Donkey anti-rat Alexa Fluor
761 555 (A78945, ThermoFisher), Donkey anti-goat Alexa Fluor 647 (A32849, ThermoFisher),
762 Donkey anti-mouse Alexa Fluor 568 (A10037, ThermoFisher) and Donkey anti-mouse Alexa
763 Fluor 647(A-31571, ThermoFisher). We stained samples with primary and secondary
764 antibodies overnight at a 1:1000 dilution in PBST (0.1 % Tween™ 20) containing 1 % Bovine
765 Serum Albumin (Biowest, P6154).

766

767 ***In situ* hybridization and hybridization chain reaction**

768 Probe generation and *in situ* hybridization were described previously[18]. Probes against Axin2,
769 Dusp4, Hes7 and Lfng were used as described in the literature[18,82,83]. Probes against Achilles
770 and Hes1 were generated using the full-length cDNA[84]. Subsequently samples were
771 dehydrated, paraffin embedded, and sectioned. Standard H&E staining was performed.

Hybridization chain reaction was performed as described previously[62]. Probe sets for the following gene targets: Dll1, Dll3, Dll4, Hes5, Hes7, Meox1, Notch1, Notch2, Notch3, Notch4 and Pax6 were used. All animals for HCR were stained once using the same hybridization, washing and amplification time for all gene targets.

Images of ISHs were taken with a Leica M165 FC stereo-microscope using 8:1 zoom. Images of HCR were taken with a Leica TCS SP8 MP confocal microscope using a 10x and 20x objective (details below). Brightness and contrast were adjusted uniformly to the entire image.

Confocal microscopy

Imaging was performed using a Leica TCS SP8 MP confocal microscope featuring an incubator and gas mixer for CO_2, O_2 and temperature control. Samples were excited with a OPSL Laser at a wavelength of 514 nm (Hes1-Achilles, Achilles-Hes7 and LuVeLu) or 568 nm (H2B-mCherry) or 638 nm (Sox2-iRFP) through a HC PL APO CS2 20x/0.75 DRY objective. For *ex vivo* culture experiments, a z-stack of 10-12 planes at 10 µm distance was scanned every 10 min. For *in vitro* differentiation experiments, a z-stack of 3-4 planes at 5 µm distance was scanned every 5 min. Multiple samples were recorded using a motorized stage during each experiment. Movies were recorded in 512 x 512 pixels (pixel size 1,517 µm). For imaging of immunostaining and HCR samples, a z-stack of 10-12 planes at 10 µm distance was scanned in 1024 x 1024 pixels (pixel size 0,758 µm).

QUANTIFICATION AND STATISTICAL ANALYSIS

Image and data processing

For quantification of mean intensity or number of positive cells in fixed sample imaging, Fiji[85] was used. Kymographs were generated as described previously[68]. For quantification of mean intensity over time, ROImanager, Mastodon or manual tracking were used. Quantification of oscillation dynamics were performed using pyBOAT[47] and Julia. For determination of main period and amplitude, sample tracks were averaged and normalised (either by mean or DMSO, as stated in the legends) using Julia. Furthermore, all graphs and heatmaps are plotted using Julia.

Statistical analysis

For all experiments at least three independent experiments were performed. To visualize data, Tukey style boxplots were used (bar=median, box=25th and 75th percentile, whiskers=1.5*IQR). Data displayed as violin plots present data from max to min with bar=median. For statistical comparisons between groups, Mann-Whitney U tests were computed in Julia.

DATA AND SOFTWARE AVAILABILITY

Julia scripts are available upon request.

KEY RESOURCES TABLE

REAGENT or RESOURCE	SOURCE	IDENTIFIER
Antibodies		
anti-Dll1 rat	Sigma-Aldrich	MABN2284
anti-Dll4 goat	R&D Systems	AF1389-SP
anti-Cleaved Caspase-3 rabbit	CST	9661S
anti-phospho Histone H3 mouse	Sigma-Aldrich	05-806
Alexa Fluor 555 Phalloidin	ThermoFisher	A34055
anti-Tbx6 rabbit	Abcam	ab38883
anti-Sox2 mouse	Abcam	ab79351
anti-Sox2 rabbit	Abcam	ab92494
anti-T human/mouse	R&D Systems	AF2085-SP
anti-Pax6 recombinant	Abcam	ab195045
Goat anti-Rat Alexa Fluor 555	ThermoFisher	A-21434
Donkey anti-Rabbit Alexa Fluor 488	ThermoFisher	A-21206
Donkey anti-Rabbit Alexa Fluor 568	ThermoFisher	A10042
Donkey anti-rabbit Alexa Fluor 405	ThermoFisher	A48258
Donkey anti-mouse Alexa Fluor 647	ThermoFisher	A-31571
Donkey anti-mouse Alexa Fluor 568	ThermoFisher	A10037
and Donkey anti-mouse Alexa Fluor 647	ThermoFisher	A-31571
Bacterial and Virus Strains		
N/A	N/A	N/A

Biological Samples		
N/A	N/A	N/A
Chemicals, Peptides, and Recombinant Proteins		
OneTaq® Quick-Load® 2X Master Mix with Standard Buffer	New England Biolabs	M0486L
DAPT	Sigma-Aldrich	D5942
IWP-2	Sigma-Aldrich	I0536
SU5402	Sigma-Aldrich	SML0443
CHIR99021	Sigma-Aldrich	SML1046
PD0325901	MedChemExpress	HY-10254
FGF-basic	Prepotech	450-33
Retinoic acid	Sigma-Aldrich	R2625-50MG
DAPI	Sigma-Aldrich	D9542-10MG
DMEM/F-12, no phenol red	Gibco	21041025
Special medium DMEM/F-12, without glucose, glutamine, pyruvate and phenol red	Cell Culture Technologies	N/A
Special Advanced DMEM/F-12, without phenol red, glutamine, albumin, transferrin and insulin	Cell Culture Technologies	N/A
Insulin, Human Recombinant	Millipore	91077C-100MG
holo-Transferrin human	Sigma-Aldrich	T0665-50MG
AlbuMAX™ II Lipid-Rich BSA	Gibco	11021029
Neurobasal™ Medium, minus phenol red	Gibco	12348017
N-2 Supplement (100X)	Gibco	17502048
B-27™ Supplement (50X), minus vitamin A	Gibco	12587010
B-27™ Supplement (50X), minus antioxidants	Gibco	10889038
GlutaMAX™ Supplement	Gibco	35050038
Glucose Solution 45	Sigma-Aldrich	G8769
LIF	Sigma-Aldrich	PD0325901
Bovine Serum Albumin (BSA)	Biowest	P6154
KnockOut™ Serum Replacement (KSR)	Gibco	10828028
2-Mercaptoethanol	Gibco	21985023
Penicillin-Streptomycin	Gibco	15140122
Lipofectamine 3000	ThermoFisher	L3000001

Fibronectin	Sigma-Aldrich	F1141
Tamoxifen	Sigma-Aldrich	T5648-1G
8-well Chambered Coverglass w/ non-removable wells	ThermoFisher	155411PK
μ-Dish 35 mm Quad	Ibidi	80416
Critical Commercial Assays		
N/A	N/A	N/A
Deposited Data		
N/A	N/A	N/A
Experimental Models: mouse ESC lines		
Hes1-Achilles_RosaCreERT_Sox2-iRFP	This paper	N/A
Experimental Models: Organisms/Strains		
Mouse: Hes1-Achilles	This paper	N/A
Mouse: Achilles-Hes7	Yoshioka-Kobayashi et al., 2020	N/A
Mouse: LuVeLu:CD1-Tg(Lfng-YFP/PEST)OP	Aulehla et al., 2008	N/A
Mouse: R26R-H2B-mCherry	Ventura et al., 2007	N/A
Mouse: Tg(T-cre/ERT2)1Lwd/J	Lallemand et al., 1998	N/A
Mouse: Tg(Pgk1-cre)1Lni/CrsJ	Glynn et al., 2006	N/A
Mouse: R26-CreERT2	Schindelin et al., 2012	N/A
Oligonucleotides		
Hes1-C-forward: GACCTCGGTGGGTCCTAACGC	This paper	N/A
Linker-Achilles-reverse: CTTGCCGGTGGTGCAGATCAG	This paper	N/A
Hes1-N-reverse: GAGGTGGGCTAGGGACTTTACGG	This paper	N/A

Recombinant DNA		
N/A	N/A	N/A
Software and Algorithms		
Fiji	Schindelin et al., 2012	https://fiji.sc/
insitu_probe_generator	N/A	https://github.com/rwnull/insitu_probe_generator
Mastodon	N/A	https://github.com/mastodon-sc
Pyboat	Mönke et al., 2020	https://github.com/tensionhead/pyBOAT
Julia	N/A	https://julialang.org/
Other		
M165 FC	Leica	N/A
SP8MP	Leica	N/A

Supplemental Information

The supplemental material contains 7 supplemental figures, 2 movies and 1 file containing timeseries data.

References

1. Sonnen, K.F., and Janda, C.Y. (2021). Signalling dynamics in embryonic development. Biochem J *478*, 4045-4070. 10.1042/BCJ20210043.
2. Sasai, Y., Kageyama, R., Tagawa, Y., Shigemoto, R., and Nakanishi, S. (1992). Two mammalian helix-loop-helix factors structurally related to Drosophila hairy and Enhancer of split. Genes Dev *6*, 2620-2634. 10.1101/gad.6.12b.2620.
3. Ohtsuka, T., Ishibashi, M., Gradwohl, G., Nakanishi, S., Guillemot, F., and Kageyama, R. (1999). Hes1 and Hes5 as notch effectors in mammalian neuronal differentiation. EMBO J. *18*, 2196-2207. 10.1093/emboj/18.8.2196.

4. Palmeirim, I., Henrique, D., Ish-Horowicz, D., and Pourquié, O. (1997). Avian hairy gene expression identifies a molecular clock linked to vertebrate segmentation and somitogenesis. Cell *91*, 639-648. papers2://publication/uuid/48EC5D4B-3F1C-41E5-9D97-1E585DFC58EC.
5. Wu, Y., Liu, Y., Levine, E.M., and Rao, M.S. (2003). Hes1 but not Hes5 regulates an astrocyte versus oligodendrocyte fate choice in glial restricted precursors. Developmental dynamics *226*, 675-689. papers2://publication/uuid/DA4709A1-DF9F-418E-9D1D-027F46335FE0.
6. Ohtsuka, T., Sakamoto, M., Guillemot, F., and Kageyama, R. (2001). Roles of the basic helix-loop-helix genes Hes1 and Hes5 in expansion of neural stem cells of the developing brain. J. Biol. Chem. *276*, 30467-30474. papers2://publication/doi/10.1074/jbc.M102420200.
7. Kobayashi, T., and Kageyama, R. (2010). Hes1 regulates embryonic stem cell differentiation by suppressing Notch signaling. Genes to Cells *15*, 689-698. 10.1111/j.1365-2443.2010.01413.x.
8. Cambray, N., and Wilson, V. (2002). Axial progenitors with extensive potency are localised to the mouse chordoneural hinge. Development *129*, 4855-4866. papers2://publication/uuid/54A7EB61-2FEB-4B55-8483-39FECDE61AC7.
9. Cambray, N., and Wilson, V. (2007). Two distinct sources for a population of maturing axial progenitors. Development *134*, 2829-2840. papers2://publication/doi/10.1242/dev.02877.
10. Wilson, V., Olivera-Martinez, I., and Storey, K.G. (2009). Stem cells, signals and vertebrate body axis extension. Development *136*, 1591-1604. papers2://publication/doi/10.1242/dev.021246.
11. Shimojo, H., Isomura, A., Ohtsuka, T., Kori, H., Miyachi, H., and Kageyama, R. (2016). Oscillatory control of Delta-like1 in cell interactions regulates dynamic gene expression and tissue morphogenesis. Genes Dev *30*, 102-116. 10.1101/gad.270785.115.
12. Shimojo, H., Ohtsuka, T., and Kageyama, R. (2008). Oscillations in notch signaling regulate maintenance of neural progenitors. Neuron *58*, 52-64. papers2://publication/doi/10.1016/j.neuron.2008.02.014.
13. Hirata, H., Yoshiura, S., Ohtsuka, T., Bessho, Y., Harada, T., Yoshikawa, K., and Kageyama, R. (2002). Oscillatory expression of the bHLH factor Hes1 regulated by a negative feedback loop. Science *298*, 840-843. papers2://publication/doi/10.1126/science.1074560.
14. Bosman, S.L., and Sonnen, K.F. (2022). Signaling oscillations in embryonic development. Curr Top Dev Biol *149*, 341-372. 10.1016/bs.ctdb.2022.02.011.
15. Dequéant, M.L., Glynn, E., Gaudenz, K., Wahl, M., Chen, J., Mushegian, A., and Pourquie, O. (2006). A complex oscillating network of signaling genes underlies the mouse segmentation clock. Science *314*, 1595-1598.
16. Matsuda, M., Yamanaka, Y., Uemura, M., Osawa, M., Saito, M.K., Nagahashi, A., Nishio, M., Guo, L., Ikegawa, S., Sakurai, S., et al. (2020). Recapitulating the human segmentation clock with pluripotent stem cells. Nature *580*, 124-129. 10.1038/s41586-020-2144-9.
17. Niwa, Y., Shimojo, H., Isomura, A., Gonzalez, A., Miyachi, H., and Kageyama, R. (2011). Different types of oscillations in Notch and Fgf signaling regulate the spatiotemporal periodicity of somitogenesis. Genes Dev *25*, 1115-1120. 10.1101/gad.2035311.

10.1101/gad.2035311.

18. Aulehla, A., Wehrle, C., Brand-Saberi, B., Kemler, R., Gossler, A., Kanzler, B., and Herrmann, B.G. (2003). Wnt3a plays a major role in the segmentation clock controlling somitogenesis. Developmental cell *4*, 395-406. papers2://publication/uuid/E5FEF525-1C32-4874-9DEC-78F2097E48DA.
19. Riedel-Kruse, I.H., Müller, C., and Oates, A.C. (2007). Synchrony dynamics during initiation, failure, and rescue of the segmentation clock. Science *317*, 1911-1915. papers2://publication/doi/10.1126/science.1142538.
20. Soza-Ried, C., Ozturk, E., Ish-Horowicz, D., and Lewis, J. (2014). Pulses of Notch activation synchronise oscillating somite cells and entrain the zebrafish segmentation clock. Development *141*, 1780-1788. 141/8/1780 [pii]

10.1242/dev.102111.
21. Oginuma, M., Takahashi, Y., Kitajima, S., Kiso, M., Kanno, J., Kimura, A., and Saga, Y. (2010). The oscillation of Notch activation, but not its boundary, is required for somite border formation and rostral-caudal patterning within a somite. Development *137*, 1515-1522. dev.044545 [pii]

10.1242/dev.044545.
22. Venzin, O.F., and Oates, A.C. (2020). What are you synching about? Emerging complexity of Notch signaling in the segmentation clock. Dev. Biol. *460*, 40-54. 10.1016/j.ydbio.2019.06.024.
23. Holley, S.A., Julich, D., Rauch, G.J., Geisler, R., and Nusslein-Volhard, C. (2002). her1 and the notch pathway function within the oscillator mechanism that regulates zebrafish somitogenesis. Development *129*, 1175-1183. 10.1242/dev.129.5.1175.
24. Bessho, Y., Sakata, R., Komatsu, S., Shiota, K., Yamada, S., and Kageyama, R. (2001). Dynamic expression and essential functions of Hes7 in somite segmentation. Genes & ,Ä¶ *15*, 2642-2647. papers2://publication/doi/10.1101/gad.930601.
25. Delfino-Machin, M., Lunn, J.S., Breitkreuz, D.N., Akai, J., and Storey, K.G. (2005). Specification and maintenance of the spinal cord stem zone. Development *132*, 4273-4283. 10.1242/dev.02009.
26. Akai, J., Halley, P.A., and Storey, K.G. (2005). FGF-dependent Notch signaling maintains the spinal cord stem zone. Genes Dev *19*, 2877-2887. 10.1101/gad.357705.
27. Semprich, C.I., Davidson, L., Amorim Torres, A., Patel, H., Briscoe, J., Metzis, V., and Storey, K.G. (2022). ERK1/2 signalling dynamics promote neural differentiation by regulating chromatin accessibility and the polycomb repressive complex. PLoS Biol *20*, e3000221. 10.1371/journal.pbio.3000221.
28. Manning, C.S., Biga, V., Boyd, J., Kursawe, J., Ymisson, B., Spiller, D.G., Sanderson, C.M., Galla, T., Rattray, M., and Papalopulu, N. (2019). Quantitative single-cell live imaging links HES5 dynamics with cell-state and fate in murine neurogenesis. Nat. Commun. *10*, 1-19. 10.1038/s41467-019-10734-8

10.1038/s41467-019-10734-8.
29. Biga, V., Hawley, J., Soto, X., Johns, E., Han, D., Bennett, H., Adamson, A.D., Kursawe, J., Glendinning, P., Manning, C.S., and Papalopulu, N. (2021). A dynamic, spatially periodic, micro-pattern of HES5 underlies neurogenesis in the mouse spinal cord. Mol. Syst. Biol. *17*, e9902. 10.15252/msb.20209902.
30. Imayoshi, I., and Kageyama, R. (2014). bHLH factors in self-renewal, multipotency, and fate choice of neural progenitor cells. Neuron *82*, 9-23. 10.1016/j.neuron.2014.03.018.
31. Marinopoulou, E., Biga, V., Sabherwal, N., Miller, A., Desai, J., Adamson, A.D., and Papalopulu, N. (2021). HES1 protein oscillations are necessary for neural stem cells to exit from quiescence. iScience *24*, 103198. 10.1016/j.isci.2021.103198.
32. Sueda, R., Imayoshi, I., Harima, Y., and Kageyama, R. (2019). High Hes1 expression and resultant Ascl1 suppression regulate quiescent vs. active neural stem cells in the adult mouse brain. Genes Dev *33*, 511-523. 10.1101/gad.323196.118.
33. Morales, A.V., Yasuda, Y., and Ish-Horowicz, D. (2002). Periodic Lunatic fringe expression is controlled during segmentation by a cyclic transcriptional enhancer responsive to notch signaling. Developmental cell *3*, 63-74. papers2://publication/uuid/7F38E81D-F29F-4398-8F9A-8CE4211075F5.
34. Lázaro, J., Costanzo, M., Sanaki-Matsumiya, M., Girardot, C., Hayashi, M., Hayashi, K., Diecke, S., Hildebrandt, T.B., Lazzari, G., Wu, J., et al. (2022). A stem cell zoo uncovers intracellular scaling of developmental tempo across mammals. bioRxiv, 2022.2010.2013.512072. 10.1101/2022.10.13.512072.
35. Harima, Y., Takashima, Y., Ueda, Y., Ohtsuka, T., and Kageyama, R. (2013). Accelerating the tempo of the segmentation clock by reducing the number of introns in the Hes7 gene. Cell Rep *3*, 1-7. papers2://publication/doi/10.1016/j.celrep.2012.11.012.

36. Bessho, Y., Hirata, H., Masamizu, Y., and Kageyama, R. (2003). Periodic repression by the bHLH factor Hes7 is an essential mechanism for the somite segmentation clock. Genes Dev *17*, 1451-1456. 10.1101/gad.1092303.
37. Diaz-Cuadros, M., Wagner, D.E., Budjan, C., Hubaud, A., Tarazona, O.A., Donelly, S., Michaut, A., Al Tanoury, Z., Yoshioka-Kobayashi, K., Niino, Y., et al. (2020). In vitro characterization of the human segmentation clock. Nature *580*, 113-118. 10.1038/s41586-019-1885-9.
38. Yoshioka-Kobayashi, K., Matsumiya, M., Niino, Y., Isomura, A., Kori, H., Miyawaki, A., and Kageyama, R. (2020). Coupling delay controls synchronized oscillation in the segmentation clock. Nature *580*, 119-123. 10.1038/s41586-019-1882-z.
39. Niwa, Y., Masamizu, Y., Liu, T., Nakayama, R., Deng, C.-X., and Kageyama, R. (2007). The initiation and propagation of Hes7 oscillation are cooperatively regulated by Fgf and notch signaling in the somite segmentation clock. Developmental cell *13*, 298-304. papers2://publication/doi/10.1016/j.devcel.2007.07.013.
40. Masamizu, Y., Ohtsuka, T., Takashima, Y., Nagahara, H., Takenaka, Y., Yoshikawa, K., Okamura, H., and Kageyama, R. (2006). Real-time imaging of the somite segmentation clock: revelation of unstable oscillators in the individual presomitic mesoderm cells. Proc. Natl. Acad. Sci. U. S. A. *103*, 1313-1318. papers2://publication/doi/10.1073/pnas.0508658103.
41. Jennings, B.H., Pickles, L.M., Wainwright, S.M., Roe, S.M., Pearl, L.H., and Ish-Horowicz, D. (2006). Molecular recognition of transcriptional repressor motifs by the WD domain of the Groucho/TLE corepressor. Mol Cell *22*, 645-655. 10.1016/j.molcel.2006.04.024.
42. Fisher, A.L., Ohsako, S., and Caudy, M. (1996). The WRPW motif of the hairy-related basic helix-loop-helix repressor proteins acts as a 4-amino-acid transcription repression and protein-protein interaction domain. Mol Cell Biol *16*, 2670-2677. 10.1128/MCB.16.6.2670.
43. Jumper, J., Evans, R., Pritzel, A., Green, T., Figurnov, M., Ronneberger, O., Tunyasuvunakool, K., Bates, R., Zidek, A., Potapenko, A., et al. (2021). Highly accurate protein structure prediction with AlphaFold. Nature *596*, 583-589. 10.1038/s41586-021-03819-2.
44. Bulusu, V., Prior, N., Snaebjornsson, M.T., Kuehne, A., Sonnen, K.F., Kress, J., Stein, F., Schultz, C., Sauer, U., and Aulehla, A. (2017). Spatiotemporal Analysis of a Glycolytic Activity Gradient Linked to Mouse Embryo Mesoderm Development. Dev Cell *40*, 331-341 e334. 10.1016/j.devcel.2017.01.015.
45. Lauschke, V.M., Tsiairis, C.D., Francois, P., and Aulehla, A. (2013). Scaling of embryonic patterning based on phase-gradient encoding. Nature *493*, 101-105. papers2://publication/doi/10.1038/nature11804.
46. Aulehla, A., Wiegraebe, W., Baubet, V., Wahl, M.B., Deng, C., Taketo, M., Lewandoski, M., and Pourquié, O. (2008). A beta-catenin gradient links the clock and wavefront systems in mouse embryo segmentation. Nat Cell Biol *10*, 186-193. 10.1038/ncb1679.
47. Mönke, G., Sorgenfrei, F.A., Schmal, C., and Granada, A.E. (2020). Optimal time frequency analysis for biological data - pyBOAT. bioRxiv, 2020.2004.2029.067744. 10.1101/2020.04.29.067744.
48. Gouti, M., Tsakiridis, A., Wymeersch, F.J., Huang, Y.L., Kleinjung, J., Wilson, V., and Briscoe, J. (2014). In Vitro Generation of Neuromesodermal Progenitors Reveals Distinct Roles for Wnt Signalling in the Specification of Spinal Cord and Paraxial Mesoderm Identity. PLoS Biol. *12*. ARTN e1001937

10.1371/journal.pbio.1001937.
49. Schmid-Burgk, J.L., Honing, K., Ebert, T.S., and Hornung, V. (2016). CRISPaint allows modular base-specific gene tagging using a ligase-4-dependent mechanism. Nat Commun *7*, 12338. 10.1038/ncomms12338.
50. Metzis, V., Steinhauser, S., Pakanavicius, E., Gouti, M., Stamataki, D., Ivanovitch, K., Watson, T., Rayon, T., Mousavy Gharavy, S.N., Lovell-Badge, R., et al. (2018). Nervous System Regionalization Entails Axial Allocation before Neural Differentiation. Cell *175*, 1105-1118 e1117. 10.1016/j.cell.2018.09.040.

51. Bansod, S., Kageyama, R., and Ohtsuka, T. (2017). Hes5 regulates the transition timing of neurogenesis and gliogenesis in mammalian neocortical development. Development *144*, 3156-3167. 10.1242/dev.147256.
52. Patel, N.S., Rhinn, M., Semprich, C.I., Halley, P.A., Dolle, P., Bickmore, W.A., and Storey, K.G. (2013). FGF signalling regulates chromatin organisation during neural differentiation via mechanisms that can be uncoupled from transcription. Plos Genet *9*, e1003614. 10.1371/journal.pgen.1003614.
53. Dubrulle, J., and Pourquié, O. (2004). fgf8 mRNA decay establishes a gradient that couples axial elongation to patterning in the vertebrate embryo. Nature *427*, 419-422. papers2://publication/doi/10.1038/nature02216.
54. Dubrulle, J., McGrew, M.J., and Pourquié, O. (2001). FGF signaling controls somite boundary position and regulates segmentation clock control of spatiotemporal Hox gene activation. Cell *106*, 219-232. papers2://publication/uuid/D59005F9-BA4E-4ABA-8994-0E3B26A4CF15.
55. Goodwin, B.C. (1965). Oscillatory behavior in enzymatic control processes. Adv. Enzyme Regul. *3*, 425-438. papers2://publication/uuid/C3F9BC22-AA48-45A5-A2E5-935074E285C2.
56. Monk, N.A. (2003). Oscillatory Expression of Hes1, p53, and NF-kB Driven by Transcriptional Time Delays. Curr Biol *13*. papers2://publication/uuid/8C8BF869-F4D5-4D00-826B-475EA61AEFD1.
57. Takashima, Y., Ohtsuka, T., González, A., Miyachi, H., and Kageyama, R. (2011). Intronic delay is essential for oscillatory expression in the segmentation clock. Proc. Natl. Acad. Sci. U.S.A. *108*, 3300-3305. papers2://publication/doi/10.1073/pnas.1014418108.
58. Freeman, M. (2000). Feedback control of intercellular signalling in development. Nature *408*, 313-319. 10.1038/35042500.
59. Takagi, A., Isomura, A., Yoshioka-Kobayashi, K., and Kageyama, R. (2020). Dynamic Delta-like1 expression in presomitic mesoderm cells during somite segmentation. Gene Expr Patterns *35*, 119094. 10.1016/j.gep.2019.119094.
60. Murray, P.J., Maini, P.K., and Baker, R.E. (2013). Modelling Delta-Notch perturbations during zebrafish somitogenesis. Dev. Biol. *373*, 407-421. papers2://publication/doi/10.1016/j.ydbio.2012.10.014.
61. Morelli, L.G., Ares, S., Herrgen, L., Schröter, C., Jülicher, F., and Oates, A.C. (2009). Delayed coupling theory of vertebrate segmentation. HFSP J *3*, 55-66. papers2://publication/doi/10.2976/1.3027088.
62. Choi, H.M.T., Schwarzkopf, M., Fornace, M.E., Acharya, A., Artavanis, G., Stegmaier, J., Cunha, A., and Pierce, N.A. (2018). Third-generation in situ hybridization chain reaction: multiplexed, quantitative, sensitive, versatile, robust. Development *145*. 10.1242/dev.165753.
63. Ferjentsik, Z., Hayashi, S., Dale, J.K., Bessho, Y., Herreman, A., De Strooper, B., del Monte, G., de la Pompa, J.L., and Maroto, M. (2009). Notch is a critical component of the mouse somitogenesis oscillator and is essential for the formation of the somites. Plos Genet *5*, e1000662. papers2://publication/doi/10.1371/journal.pgen.1000662.
64. Özbudak, E.M., and Lewis, J. (2008). Notch signalling synchronizes the zebrafish segmentation clock but is not needed to create somite boundaries. Plos Genet *4*, e15. papers2://publication/doi/10.1371/journal.pgen.0040015.
65. Horikawa, K., Ishimatsu, K., Yoshimoto, E., Kondo, S., and Takeda, H. (2006). Noise-resistant and synchronized oscillation of the segmentation clock. Nature *441*, 719-723. papers2://publication/doi/10.1038/nature04861.
66. Evrard, Y.A., Lun, Y., Aulehla, A., Gan, L., and Johnson, R.L. (1998). lunatic fringe is an essential mediator of somite segmentation and patterning. Nature *394*, 377-381. 10.1038/28632.
67. Maeda, Y., Isomura, A., Masaki, T., and Kageyama, R. (2023). Differential cell-cycle control by oscillatory versus sustained Hes1 expression via p21. Cell Rep *42*, 112520. 10.1016/j.celrep.2023.112520.

68. Sonnen, K.F., Lauschke, V.M., Uraji, J., Falk, H.J., Petersen, Y., Funk, M.C., Beaupeux, M., François, P., Merten, C.A., and Aulehla, A. (2018). Modulation of Phase Shift between Wnt and Notch Signaling Oscillations Controls Mesoderm Segmentation. Cell *172*, 1079-1090.e1012. 10.1016/j.cell.2018.01.026.
69. Seymour, P.A., Collin, C.A., Egeskov-Madsen, A.R., Jorgensen, M.C., Shimojo, H., Imayoshi, I., de Lichtenberg, K.H., Kopan, R., Kageyama, R., and Serup, P. (2020). Jag1 Modulates an Oscillatory Dll1-Notch-Hes1 Signaling Module to Coordinate Growth and Fate of Pancreatic Progenitors. Dev. Cell *52*, 731-747 e738. 10.1016/j.devcel.2020.01.015

10.1016/j.devcel.2020.01.015. Epub 2020 Feb 13.
70. Zhang, Y., Lahmann, I., Baum, K., Shimojo, H., Mourikis, P., Wolf, J., Kageyama, R., and Birchmeier, C. (2021). Oscillations of Delta-like1 regulate the balance between differentiation and maintenance of muscle stem cells. Nat Commun *12*, 1318. 10.1038/s41467-021-21631-4.
71. Nandagopal, N., Santat, L.A., LeBon, L., Sprinzak, D., Bronner, M.E., and Elowitz, M.B. (2018). Dynamic Ligand Discrimination in the Notch Signaling Pathway. Cell *172*, 869-880.e819. 10.1016/j.cell.2018.01.002.
72. Herrgen, L., Ares, S., Morelli, L.G., Schröter, C., Jülicher, F., and Oates, A.C. (2010). Intercellular coupling regulates the period of the segmentation clock. Curr Biol *20*, 1244-1253. papers2://publication/doi/10.1016/j.cub.2010.06.034.
73. Hawley, J., Manning, C., Biga, V., Glendinning, P., and Papalopulu, N. (2022). Dynamic switching of lateral inhibition spatial patterns. Journal of the Royal Society, Interface *19*, 20220339. 10.1098/rsif.2022.0339.
74. Kobayashi, T., Mizuno, H., Imayoshi, I., Furusawa, C., Shirahige, K., and Kageyama, R. (2009). The cyclic gene Hes1 contributes to diverse differentiation responses of embryonic stem cells. Genes & ,Ä¶ *23*, 1870-1875. papers2://publication/doi/10.1101/gad.1823109.
75. Rohde, L.A., Bercowsky-Rama, A., Negrete, J., Valentin, G., Naganathan, S.R., Desai, R.A., Strnad, P., Soroldoni, D., Jülicher, F., and Oates, A.C. (2021). Cell-autonomous generation of the wave pattern within the vertebrate segmentation clock. bioRxiv, 1-15. 10.1101/2021.05.29.446196.
76. Kuan, C.Y., Tannahill, D., Cook, G.M., and Keynes, R.J. (2004). Somite polarity and segmental patterning of the peripheral nervous system. Mech Dev *121*, 1055-1068. 10.1016/j.mod.2004.05.001.
77. Lallemand, Y., Luria, V., Haffner-Krausz, R., and Lonai, P. (1998). Maternally expressed PGK-Cre transgene as a tool for early and uniform activation of the Cre site-specific recombinase. Transgenic Res *7*, 105-112. 10.1023/a:1008868325009.
78. Abe, T., Kiyonari, H., Shioi, G., Inoue, K.-I., Nakao, K., Aizawa, S., and Fujimori, T. (2011). Establishment of conditional reporter mouse lines at ROSA26 locus for live cell imaging. Genesis *49*, 579-590. papers2://publication/doi/10.1002/dvg.20753.
79. Anderson, M.J., Naiche, L.A., Wilson, C.P., Elder, C., Swing, D.A., and Lewandoski, M. (2013). TCreERT2, a transgenic mouse line for temporal control of Cre-mediated recombination in lineages emerging from the primitive streak or tail bud. PLoS ONE *8*, e62479. 10.1371/journal.pone.0062479.
80. Ventura, A., Kirsch, D.G., McLaughlin, M.E., Tuveson, D.A., Grimm, J., Lintault, L., Newman, J., Reczek, E.E., Weissleder, R., and Jacks, T. (2007). Restoration of p53 function leads to tumour regression in vivo. Nature *445*, 661-665. 10.1038/nature05541.
81. Silva, J., Barrandon, O., Nichols, J., Kawaguchi, J., Theunissen, T.W., and Smith, A. (2008). Promotion of reprogramming to ground state pluripotency by signal inhibition. PLoS Biol *6*, e253. 10.1371/journal.pbio.0060253.
82. Mansouri, A., Yokota, Y., Wehr, R., Copeland, N.G., Jenkins, N.A., and Gruss, P. (1997). Paired-related murine homeobox gene expressed in the developing sclerotome, kidney, and nervous system. Dev Dyn *210*, 53-65. 10.1002/(SICI)1097-0177(199709)210:1<53::AID-AJA6>3.0.CO;2-0.

83. Saga, Y., Hata, N., Koseki, H., and Taketo, M.M. (1997). Mesp2: a novel mouse gene expressed in the presegmented mesoderm and essential for segmentation initiation. Genes Dev *11*, 1827-1839.
84. Morimoto, M., Sasaki, N., Oginuma, M., Kiso, M., Igarashi, K., Aizaki, K., Kanno, J., and Saga, Y. (2007). The negative regulation of Mesp2 by mouse Ripply2 is required to establish the rostro-caudal patterning within a somite. Development *134*, 1561-1569. 10.1242/dev.000836.
85. Schindelin, J., Arganda-Carreras, I., Frise, E., Kaynig, V., Longair, M., Pietzsch, T., Preibisch, S., Rueden, C., Saalfeld, S., Schmid, B., et al. (2012). Fiji: an open-source platform for biological-image analysis. Nat Methods *9*, 676-682. 10.1038/nmeth.2019.